POLYTECHNIQUE MONTRÉAL

affiliée à l'Université de Montréal

Dispersion Characterization in Single-Mode Optical Fibers
for Supercontinuum Generation Supporting Few-Cycle Pulses

BENJAMIN MAINGOT

Département de génie physique

Mémoire présenté en vue de l'obtention du diplôme de *Maîtrise ès sciences appliquées*
Génie physique

Mars 2020

POLYTECHNIQUE MONTRÉAL

affiliée à l'Université de Montréal

Ce mémoire intitulé :

Dispersion Characterization in Single-Mode Optical Fibers
for Supercontinuum Generation Supporting Few-Cycle Pulses

présenté par **Benjamin MAINGOT**
en vue de l'obtention du diplôme de *Maîtrise ès sciences appliquées*
a été dûment accepté par le jury d'examen constitué de :

Sébastien FRANCOEUR, président
Denis SELETSKIY, membre et directeur de recherche
Raman KASHYAP, membre

ACKNOWLEDGEMENTS

RÉSUMÉ

Dans les dernières décennies, le domaine de la photonique ultra rapide a connu de nombreuses avancées. Cela a été motivé du côté de l'industrie par l'augmentation de la bande passante et l'utilisation des fibres optiques pour transmettre l'information et du côté fondamental par le fait que la génération d'impulsions lumineuses courtes donne accès à un instrument d'exploration des dynamiques fondamentales de la matière. La propagation d'impulsions ultra courtes est accompagnée par un élargissement spectral induit par des effets d'optique non linéaire dus à l'intensité importante de l'impulsion. La géométrie des fibres optiques permet la propagation confinée de la lumière pour une distance supérieure à la longueur de diffraction caractéristique. Cela fait des fibres monomodes des candidates très attractives pour la génération d'impulsions à l'aide d'effets non linéaires. La propagation de telles impulsions est fortement influencée par les propriétés dispersives des matériaux et du guide d'onde et pousse l'étude des caractéristiques dispersives des fibres mono-modes à travers une large bande spectrale.

L'objectif principal du projet est de caractériser la dispersion de fibres optiques avec une extrême précision sur une large région spectrale. A cause de la dispersion induite par la géométrie du guide d'onde, utiliser l'équation de Sellmeier ne suffit pas pour décrire précisément la dispersion dans une fibre optique. Il est donc nécessaire de construire un montage optique. Un interféromètre de Mach-Zehnder qui contient la fibre sous étude dans un de ses bras et une ligne à délai dans l'autre est parfait pour cette application. L'étude des interférences à des longueurs d'onde différentes permet d'obtenir toute l'information nécessaire à l'extraction de la dispersion, comme le montre le chapitre 3.

L'interféromètre est un système sensible, le ratio signal sur bruit doit être optimisé à la fois lors de l'acquisition du signal et lors de son traitement subséquent. Nous appliquons une transformée de Hilbert pour récupérer l'enveloppe du signal oscillant, comme le montre le chapitre 4.

Notre montage est capable de mesurer et d'analyser la dispersion d'une fibre optique entre les longueurs d'onde de 1150 et 2600 nm. Il est compact et portable (en omettant la source de lumière) avec la possibilité de changer la fibre à étudier.

Obtenir les caractéristiques dispersives d'une fibre optique hautement non linéaire permet de simuler la propagation d'une impulsion lumineuse courte (60 fs) dans celle ci. En utilisant un programme Python pour modéliser à la fois les non-linéarités et les effets dispersifs de la fibre optique, on obtient la forme temporelle et spectrale de l'impulsion à la sortie de la fibre.

Simuler la propagation de l'impulsion dans la fibre et comparer les résultats expérimentaux avec les résultats théoriques permet d'évaluer la performance de la caractérisation et de la simulation.

Le résultat de ce projet est un ensemble d'outils pour concevoir et tester des fibres optiques pour diverses applications telles que la génération de supercontinuum, la compression d'impulsions et la compensation de dispersion.

ABSTRACT

Within the last few years, many advances have been made in the field of ultrafast photonics. On the technology side, this interest is motivated by increasing bandwidth requirements in telecommunications and the use of fiber optics to transmit information. On the fundamental side, production of short pulses provides an instrument for investigating fundamental dynamics underlying interacting internal degrees of freedom in matter. The propagation of ultrashort pulses often requires spectral broadening via optical nonlinear processes accessed through the high peak intensity of the pulse. Optical fiber geometry allows for propagation of localized light through distances much longer than the characteristic diffraction length. As a result, single-mode optical fibers are very attractive candidates as a nonlinear medium for the production of ultrashort pulses. Propagation of short pulses is also strongly influenced by the dispersion properties of the medium and thus motivates the study of dispersion properties of single-mode fibers across a wide spectral band.

The primary objective of this project is to characterize the dispersion in optical fibers with extreme precision over a large region of spectral bandwidth. Because of the dispersion induced by the waveguide geometry, Sellmeier's equations do not accurately describe the dispersive properties of a fiber. Building a characterization setup is then necessary. An unbalanced Mach-Zehnder interferometer with the fiber under measurement on one arm and a delay stage on the other is perfect in this case. Generating interferences with different input wavelengths gives all the information to compute the fiber dispersion as shown in chapter 3.

As interferometers are very sensitive, the signal to noise ratio can be improved by optimizing the electronics on the hardware side, and by using a Hilbert transform to retrieve the envelope of a signal on the processing side, as shown in chapter 4.

The setup built in this project is able to measure and analyse the dispersion of an optical fiber between the wavelengths of 1150 nm and 2600 nm. It is both compact and movable (minus the light source) with the possibility to change the fiber to measure.

Computing dispersion allows to simulate the propagation of an ultrashort pulse (60 fs) in a highly nonlinear fiber. Using a Python program to model both nonlinearities and the dispersion inside the fiber, we can compute the temporal shape of the output pulse and its spectrum.

In chapter 5, we compare actual spectra with simulated ones, as a check of both the characterization setup and the simulation code.

The result of the project is a set of tools to design and test fibers for a variety of applications such as supercontinuum generation, pulse compression and dispersion compensation.

TABLE OF CONTENTS

LIST OF FIGURES

LIST OF SYMBOLS AND ACRONYMS

OPA   Optical Parametric Amplifier

SPM   Self Phase Modulation

OSA   Optical Spectrum Analyser

NEP   Noise Equivalent Power

SNR   Signal to Noise Ratio

DAC   Digital to Analog Converter

HNF   Highly Nonlinear Fiber

FWHM   Full Width Half Maximum

IR   Infra Red

ZnSe   Sinc Selenide

Ge   Germanium

Pb   Lead

F   Fluorine

B   Boron

CW   Continuous Wave

FROG   Frequency-Resolved Optical Gating

SPIDER   Spectral Phase Interferometry for Direct Electric field Reconstruction

ZDW   Zero Dispersion Wavelength

LIST OF APPENDICES

CHAPTER 1   INTRODUCTION

Ultrafast photonics is a relatively new field of optics that aims to understand physics on a very short timescale. The development of mode locked lasers allows the realm of the femtosecond pulse durations to be reached. With the current technology, it is possible to study phenomena that happen on timescales of the order of a few femtoseconds. In addition, short timescales allow us to neglect sources of noise that happen much slower. A few femtoseconds is for example shorter than a typical phonon response time. A consequence of that is the possibility to interact with matter ignoring the phonon effects of the lattice. By virtue of the reciprocal relation between time and frequency, short pulses occupy a large band in the spectral domain. When an optical pulse propagates through a physical system, different spectral components of the pulse will propagate at different velocities. This arises from the fact that the refractive index, n, of the material is always frequency dependent. The consequence of dispersion, or $n(\omega)$, is in general a change in the arrival time of the pulse as well as a change in its temporal shape. Control of pulse duration therefore necessitates knowledge of the dispersion in the medium with high accuracy and over a broad selection of frequencies. Despite all these advantages, shortening the pulses comes with a lot of challenges. This work reports the construction of a setup for the characterization of dipersion in single mode optical fibers. In addition, we imlement a numerical model that simulates the propagation of an ultrashort pulse in an optical fiber.

1.1   Definitions and basic concepts

1.1.1   Dispersion

There are two types of dispersion a pulse of light experiences when propagating in an optical fiber. Material dispersion and waveguide dispersion.

Dispersion in bulk medium

Material dispersion is the result of a delayed temporal response of a material to an incoming electromagnetic field. It leads to variations of the refractive index with frequency, which is connected to the material optical resonances through the causal Kramers-Krönig relations. It is generally described by a Sellmeier equation, where $n^2(\lambda) = 1 + \sum_i \frac{B_i \lambda^2}{\lambda^2 - C_i}$ with B_i and C_i experimentally determined coefficients.

Waveguide dispersion

Waveguide dispersion is a consequence of the dielectric waveguide confinement of the optical mode, e.g. in a fiber geometry. More precisely, a finite difference of the refractive indices between the core and the cladding materials of the fiber, an optical mode is only partially contained in the core. The evanescent components in the cladding experience a different refractive index. The delocalization of the mode across core and cladding materials result in a modification of the overall, propagation-averaged refractive index experienced by light in a given mode of the waveguide. Control of the waveguide geometry allows some freedom in engineering the dispersive properties of optical fibers.

1.1.2 Pulse compression

Propagating short pulses through a dispersive element results in the fact that different spectral components of the pulse propagate through the element at different velocities. Mathematically, this can be stated by the fact that the transfer function of the fiber can be identified as : $G(\omega) = T(\omega)e^{i\phi(\omega)}$, where $T(\omega)$ and $\phi(\omega)$ are the frequency dependent amplitude and phase response of the medium. In this work we are interested in pulse propagation in transparent media, i.e. when photon energies are far detuned from single photon absorption resonances. As a result, $T(\omega)$ can be taken as frequency independent quantity. Therefore, a transform-limited pulse in the frequency domain: $E_{\text{in}}(\omega) = E_0(\omega)e^{-i\omega t}$ gets modified as $E_{\text{out}}(\omega) = E_{\text{in}}(\omega)G(\omega) = E_0(\omega)e^{-i\omega t+\phi(\omega)}$, where we assumed that $T(\omega) = 1$. Thus, propagating affects the phase relations between different frequency components of a pulse. For a given amplitude spectrum, the spectral shape of the phase affects the pulse duration. Adjusting the phase of a light pulse to reach the Fourier-limited duration is called pulse compression. For a given spectral phase of the response function we can Taylor expand it around the center frequency of interest. The first frequency-independent term is responsible for the global phase-shift of the wave, corresponding to the refractive index associated with the center frequency of the expansion. The second term of the expansion, namely $\frac{d\phi}{d\omega}$ is responsible for the refractive index experienced by the envelope of the pulse centered about the expansion region, and it is responsible for the group velocity of the pulse. The second-order term, $\frac{d^2\phi}{d\omega^2}$, is responsible for the frequency-dependent group velocity, which results in stretching of the pulse envelope in time, as different frequencies exhibit different velocities. This is called Group Velocity Dispersion (GVD). Higher order dispersion are responsible for more subtle effects, e.g. a third-order term will tend to provide small satellite pulses in time domain for a reasonably smooth shape of the spectral envelope of the pulse. Figure 1.1 illustrates the effect of a constant, linear and quadratic phase on pulse duration.
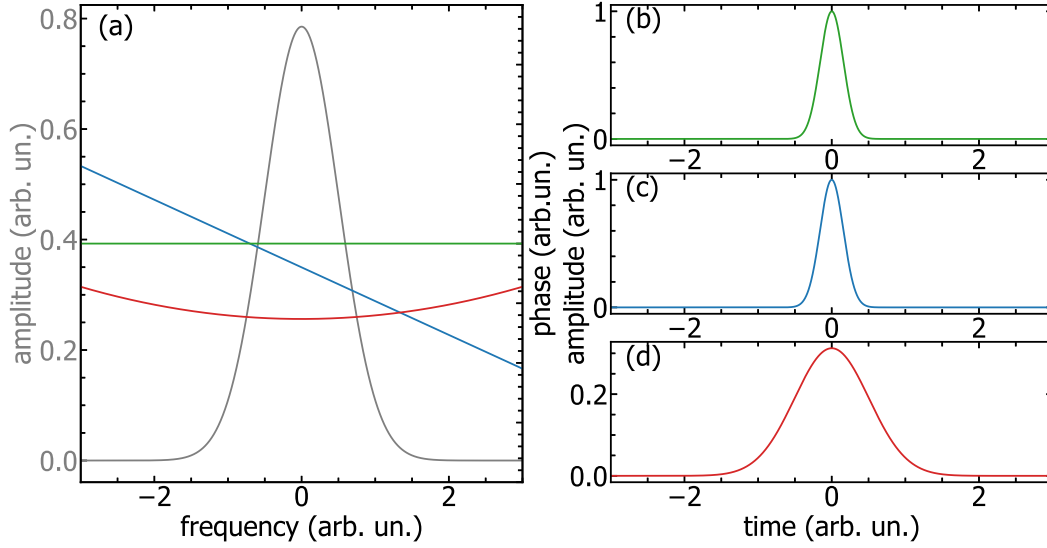
Figure 1.1 (a) Calculated pulse with a Gaussian amplitude (grey) in the Fourier domain. The green, blue and red curves correspond to constant, linear and quadratic phase profiles, respectively. Figures (b), (c) qnd (d) show the inverse Fourier transform of the Gaussian amplitude with a constant phase (b), with a linear phase (c) and with a quadratic phase (d).

1.1.3 Nonlinearities and supercontinuum

For a given pulse energy, shortening its duration means increasing the peak intensity. At sufficient peak intensity (e.g. MW/cm^2) the response of electrons to an applied electric component of the electromagnetic field can no longer be approximated by Hooke's law, where the restoring force on the displaced electron cloud is proportional to the displacement vector. Departures from this harmonic response result in the appearance of field-mixing terms in the polarization response. This opens the field of nonlinear optics. Nonlinear optics describes the behaviour of light when the polarization vector is not directly proportional to the electric field. With high enough intensity, nonlinear processes generate new frequencies in the light spectrum.

For instance, supercontinuum generation is the broadening of the amplitude spectrum of a light pulse through nonlinear effects.

1.2 Problem statement

Accurate modeling of supercontinuum generation in fibers supporting few- and single-cycle pulses requires knowledge of $\phi(\omega)$ to at least the 5th or 6th order in the Taylor expansion. This means that the fiber's dispersion has to be characterized over a large spectral window. Efficiently characterizing dispersion of an optical fiber means doing it across all the transmission bandwidth of the fiber, or at least over the whole region where the fiber is single mode. For example, the most used fiber in telecommunication is SMF28, based on fused silica. Its cutoff wavelength for single mode propagation is 1260 nm. The transmission of fused silica drops by 3dB from the peak value at wavelengths approaching high-frequency phonon modes, at 2.3 μm. These constraints push the necessity to characterize the dispersion of SMF28 and similar (oxide-based) fibers over a 1000-nm wide spectral range, spanning from the near to mid-IR.

1.2.1 Source requirements

The bandwidth requirements of the characterization setup puts stringent constraints on the source, namely that the spectral coverage of the source has to overlap with the targeted spectral band. This limits the choice to two categories of sources.

The first choice is a thermal (black body) emitter with a very broad emission spectrum, such as a tungsten filament source. With a white light source, specific wavelength bands have to be selected one at a time, for instance with a low resolution monochromator. A monochromator applies a narrow bandpass filter with a tunable center frequency. The narrow-band filtering from the broadband spectral distribution results in a significant lowering of the optical power per filter bandwidth. This limits the energy in use for the experiment and is detrimental to the signal to noise ratio (SNR). A filament element is also not a point source, which means it is more difficult to collimate the emission and to inject it in the interferometer as is. A possible solution is to perform a mode clean up with a pinhole of 10 μm in diameter to be able to achieve an image matching the core size of the fiber-under-test, for further coupling. This again implies a loss of power and impacts the SNR.

The second category of sources is one with a tunable wavelength, for example an optical parametric amplifier (OPA) seeded by a pulsed laser. With an OPA, most of the power can be used for each wavelength. However, using a pulsed source can create additional challenges. To get interference with a continuous wave source, the only parameter to adjust is the collinearity of the k vectors. Using a source with a wide spectral bandwidth adds the condition of the temporal overlap. Using a coherent can potentially pose limitations on the

input power, in order not to induce a nonlinear response.

1.2.2 Interferometer elements

For the same reasons as the lamp, all the elements of the interferometer need to have a broadband optical response. The mirrors are the least restrictive, as simple silver coated mirrors reflect more than 90 % of the power from wavelengths of 0.4 to 9 μm.

The beam splitters need to be chosen more carefully to achieve the same amount of reflection and transmission while having low loss across the whole spectrum. An acceptable solution is to deposit a thin layer of inconel on a barium fluorate substrate. Barium fluoride is transparent up to a wavelength of 10 μm and inconel has a flat reflection spectrum in the same region.

The beam has to be focused in the fiber and collimated out. Using a lens is not an option here, as the chromatic aberrations of the lens are inevitable. As an alternative, off axis parabolic mirrors are aberration-free and their metallic coatings ensure ultrabroadband response with minimal losses.

1.2.3 Signal to noise ratio optimization

One of the requirements of the project is the precision of the characterization. Hence, all the noise sources have to be minimized as much as possible.

In order to improve the SNR, the different sources of noise must be first identified. It can be done by monitoring the the interferometer while the stage is in the middle of the interference fringes. Taking the Fourier transform of the time-domain signal gives frequency dependent information on the noise contributions to the measurement.

A part of the noise is intrinsic to the detector itself, in this case an InGaAs photodiode. It is quantified by its noise equivalent power. The noise equivalent power is the quantity of power that gives a SNR of 1 over a bandwidth of one Hertz.

Identifying and reducing noise is one way to improve SNR, the other is to increase the signal, but it is very difficult to generate high power signals over a large bandwidth.

Finally, processing the acquired signal can improve the SNR, for instance by applying a spectral filter. Another option is to use a Lock-In Amplifier (LIA). Lock in amplification is the amplification of a signal at a specific frequency. The measured signal is multiplied by a sine function at a reference frequency and integrated over time. The average value of two sine functions with a different frequency is zero. Integrating significantly longer than the

period of the sine function gives a value close to zero. Lock-In amplification thus attenuates all the frequency components of the signal that are not at the reference frequency and hence shifts the detection process to frequencies where intrinsic $\frac{1}{f}$ noise is significantly reduced. Properly chosen reference frequency of the lock-in amplifier also allows to avoid any possible noise frequency regions of the experiment (e.g. due to beam pointing instability, vibrations etc.).

1.2.4 Simulation of pulse propagation

When propagating through a fiber, a light pulse is affected by two major phenomena, dispersion and nonlinear effects. They have to be considered when simulating the propagation. Dispersion is a frequency dependent phase shift, so it is best simulated in the frequency domain. On the other hand, nonlinearities are best simulated in the time domain. To take both effects into account, the pulse has to be Fourier transformed to apply dispersion, then inverse Fourier transformed to apply nonlinear effects on all the steps of the simulation. This method is called split-step Fourier method. We implement this method in this work to model pulse propagation through dispersion-engineered fibers to achieve maximal bandwidth in supercontinuum generation, supporting sub-10fs pulse durations.

1.3 Objectives of the project

The first objective is to design and build an effective setup to characterize the dispersion of optical fiber over a large band (between 1150 and 2600 nm).

The second objective is to use this setup to accurately find the dispersion of a highly nonlinear fiber.

The third objective is to use the dispersion curve obtained to simulate the propagation of a short pulse in the characterized fiber.

The fourth and last objective is to build the simulated setup to confirm the results of the simulation and the spectrum obtained in the laboratory.

1.4 Outline of the thesis

This thesis is divided into three parts.

The first part adresses the global theory on interferometry and the reason behind choosing an interferometer for this setup. This part will also discuss the specificity of having a broadband source and the setup design.

The second part discusses the measurement process itself, more precisely the acquisition technique, the signal processing, the SNR improvement and the results of these measurements.

The third and last chapter uses the results of the second one to simulate the propagation of a pulse in the measured fiber and compare this with the experiment built in the laboratory.

CHAPTER 2   LITERATURE REVIEW

2.1   Ultrafast optics

The ability to mode lock a laser cavity allowed the creation of pulsed laser sources [2]. Active mode locking was discovered in the sixties [3] and created sources with pulse durations that can be shorter than the nanosecond, the duration was indeed limited by the external modulator. Passive mode locking was discovered in the eighties and pushed the pulse duration to the femtosecond [4]. In the last decades, the barrier of the femtosecond was breached [5], [6]. These pulses have a duration much shorter than the response time of any electric device. They need special measurement setups to be analyzed. Two examples of that are the FROG [7] and the SPIDER [8].

2.2   Nonlinear effects

Working with ultrafast gives access to intensity high enough to make nonlinear effects significants. As the fibers are centrosymmetric, there are no second order effects. Third order is however present. Self phase modulation is one of the first nonlinear effect studied in fibers [9]. It comes from a change in the refractive index with intensity. It broadens the spectrum and can result in loss of information. It can also be used to generate pulses with a duration of dozens of femtoseconds [10].

When the energy is high enough, the spectrum broadens even more due to an effect called supercontinuum generation [11]. The energy splits into two major parts, at lower frequencies than the input, a soliton forms. A fundamental soliton is a wave that propagates while keeping the same temporal and spectral shape. It happens when the nonlinear effects exactly balance the dispersion. It happens when the pulse energy and its duration follow this relation: $E_p = \frac{2|\beta_2|}{|\gamma|\tau}$, where E_p is the pulse energy, τ is the pulse duration at $\frac{1}{e^2}$, γ is the nonlinear coefficient of the material and β_2 is the GVD of the material. When the pulse energy is the square of an integer (4, 9...) greater than the fundamental soliton energy, the pulse is a higher order soliton. Its frequency and temporal shapes are no longer constant, but periodic over the propagation.

On the other side of the pump spectrum, a dispersive wave forms. Self phase modulation is a third order nonlinear effect in time. Its equivalent in space is self focusing [12]. The change of refractive index causes intense enough light to focus in nonlinear media. This is called a Kerr lens. A Kerr lens is one of the options of passive mode locking in a laser cavity [13], [14].

2.3   Dispersion in optical fibers

2.3.1   Chromatic and waveguide dispersion

Ever since optical fibers have been a viable solution to transmit information [15], figuring out how to characterize and compensate the dispersion has been a important problem. The first component of the fiber dispersion is the simple chromatic dispersion. The discovery of chromatic dispersion in media (water or glass) dates back to ancient Egypt, but was not fully understood until Snell's law [16] was discovered. Most optical fibers designed to work in the telecommunication band are based on fused silica glass. To support guided modes, optical fibers have a step-index structure, where higher refractive-index core is surrounded by lower refractive-index cladding. Addition of germanium or lead in the core increases the nominal value of the refractive index of silica, while addition of boron or fluorine [17] lowers it. These additives modify the refractive index as well as chromatic dispersion of both core and cladding composition.

The second type of dispersion that takes place in the fiber is waveguide dispersion. It happens due to the confinement geometry of the guided optical mode. Depending on the wavelength of the guided mode, the proportion of energy propagating in the cladding is different. The effective refractive index arises from the wavelength-dependent lowering of the bulk refractive index. Obviously, the two types of dispersions are linked and significant [18]. For completeness, we mention that there also exists a possibility to engineer the dispersion of the material, for example by introducing a refractive index modulation along the propagation direction in optical fibers by means of e.g. writing a Bragg grating [19]. While highly successful in telecommunication applications, such elements do not typically support operation in the octave-spanning spectral range, here targeted for single-cycle optical pulse operation. In the context of optical fibers, a typically achieved contrast in the refractive index requires propagation lengths of at least tens of centimeters and relatively narrow-band modulation frequency to fully exploit the interference effects of the grating. While a highly efficient technique across and around the telecommunication band, it is not suitable for our application of supercontinuum generation with an octave-spanning spectrum (approx. 1000-2000 nm) in highly nonlinear fibers of only a few centimeter in length. In the following, we only refer to waveguide dispersion when we discuss structural effects on the dispersion properties of guided light.

Since the main interest of optical fibers is to propagate information and that the best way to transmit information is with pulses of light, dispersion is important to take into account in telecommunications.

Upon propagation through a medium with chromatic dispersion, a pulse of light changes its phase and as a result its temporal shape [20]. The effects of dispersion have been studied almost as soon as optical fibers started being used [21].

If the pulse input in the fiber is compressed (i.e. of a transform-limited pulse duration with a constant or linear spectral phase), dispersing it will always increase its duration. When the goal is transmitting information, a longer duration means that a lower bitrate must be implemented in order to avoid information scrambling provided the other parameters are identical.

As a result, solutions had to be designed to compensate the dispersion induced by the propagation. The first solution is to use a dispersion compensation fiber that has the reverse effect on the phase compared to the transmission fiber [22–24]. This type of fibers are ideal when propagating a signal over a long distance, they introduce an all-passive means to minimize or compensate the effects of pulse dispersion.

In a laboratory setting, where propagation over relatively short fiber lengths is intended, manually changing the phase of the pulse before or after the fiber can be enough to compensate. A simple way to do this is with an optical element possessing chromatic dispersion such as prism pairs [25], chirped mirrors [26], etc.

2.3.2 Characterization techniques

Given how important dispersion is for telecommunication, and as we will see for ultrafast physics, it must be characterized with high precision. It means measuring dispersion over a broad frequency range that can support accurate experimental extraction of the coefficients of the Taylor expansion well beyond the group velocity terms. This paper will explore the valid method of white light interferometry [27]. Using a white light source with an unbalanced interferometer allows for the measurements of the group velocity in the fiber. There are however different measurement techniques [28].

One possible technique to measure the dispersion in the fiber is rooted in the time domain. A "time of flight" measurement is performed with frequency-tunable pulsed light, where group velocity can be directly extracted from the time-of-arrival information. This technique works for relatively narrow-band pulses, long fiber lengths (accumulating appreciable temporal delay) and ultrafast photodiodes, as the best time resolution is of the order of the ps. These limitations render the technique not applicable toward the scientific goals set out in this work. This kind of technique can also be used to analyse living tissue [29].

Another type of measurement is an indirect phase measurement with a phase shift method.

This technique is called the modulation phase shift technique. In this technique, a continuous wave optical signal is amplitude modulated by a RF signal. Then after propagating through multiple meters of fibers, the RF signal phase shift is measured. Changing the optical frequency gives a wavelength dependent phase shift [30]. Due to the required length of fiber, this method is not a good option in the context of this project. The bandwidth of the modulator is also not sufficient to accommodate octave-spanning spectrum (as they are typically based on interference, e.g. electro-optic modulator utilizing Mach-Zenhnder geometry).

If the objective of the characterization is to study the multi-mode regime, optical low coherence reflectometry is another possible method [31]. This technique is also a technique based on interferometry. However, it uses the interference pattern generated by the pulse reflection at the output of the fiber. It is best suited for multi-modal fibers and it also needs longer fiber lengths (around 50 cm) and specialty fiber circulators to ensure the temporal delay between the modes is sufficient to spatially separate them.

Finally, the method of single-arm 3-wave interferometry can be used for precision characterization of the dispersion of an optical fiber [32]. This techniques uses a single arm interferometer. A high coherence source is propagated in a single mode fiber, and studying the spectrum of the interference pattern of the waves reflected at both interfaces of the fiber and on a mirror behind the fiber allows the retrieval of the fiber dispersion. This technique does not require long lengths of fiber to achieve precise characterization. However, this technique is not viable for broadband characterization, especially in the mid IR, because it requires spectral analysis of the signal.

The technique used in this work is temporal interferometry, the reason behind this choice of setup is the constraints behind the characterization. The method must indeed work for short lengths of fibers and over a large spectral bandwidth, in fact approaching and exceeding an octave.

To put this work in perspective, this interferometry technique has already been used, in the case of an all-fiber Michelson interferometer [33]. In this case however, the characterization bandwidth was between the wavelengths of 1100 nm and 1700 nm and the setup in general is less versatile toward acceptance of novel fibers for characterization. The advantage of an all-fiber interferometer is the inherent stability of the setup, however, as will be seen later in this Thesis, the demonstrated 5 fs temporal resolution in the group delay in Ref. [33] is matched in our free space implementation.

2.3.3   Simulation programs

Pairing the dispersion characterization with knowledge of the nonlinearities of a material allows the propagation of a pulse in said material to be simulated. Optical fibers are an example of simulated systems [17].

Pushing further than a single fiber, the simulation of complete optical communication system is possible [34].

These kind of simulations can also be modified to add a gain function in the propagation medium [35], making them a useful tool for fiber laser designs. On the other hand, it can model material loss, depending on the gain function.

CHAPTER 3 GENERAL INTERFEROMETRY THEORY AND SETUP DESIGN

The purpose of this chapter is to understand the measurements presented in the next chapter. The goal is to understand what will be measured and why the setup used an interferometer [27]. All the optical diagrams were made using the ComponentLibrary for Inkscape.

3.1 Interferometry

3.1.1 Perfectly balanced interferometer

In order to understand the choice of an interferometer and the information it brings, discussion on the theory of a linear and balanced interferometer is mandatory. Let's take a balanced Mach-Zhender interferometer with an adjustable delay τ in one branch as an example. A balanced interferometer is an interferometer with the same amount of dispersive elements in both branches, in this case, none. A diagram of this setup is given in Figure 3.1.
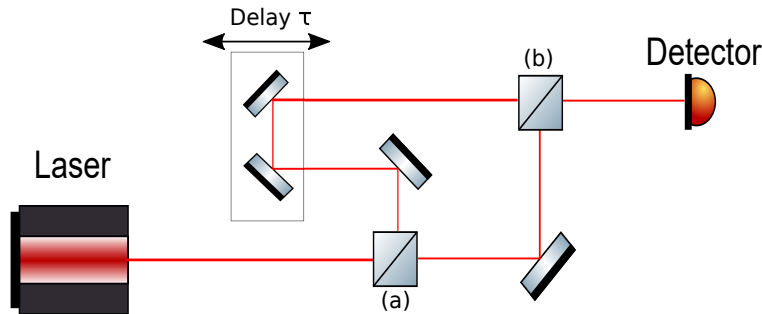
Figure 3.1 Balanced Mach-Zehnder interferometer. The laser light is split into two branches using a beam splitter (a). One of the branches has an adjustable delay τ. The beams are recombined with a second beam splitter (b) on the detector.

Let's take a look at the intensity on the detector as a function of the delay τ. We will start by introducing a couple of notations to describe the electric fields in the individual branches and the intensity observed by the detector.

The electric field in the delayed branch is $E_1(t - \tau)$ and the one in the other branch is $E_2(t)$. The complex amplitudes of these fields are $A_1(t - \tau)$ and $A_2(t)$ respectively. Finally, the intensity on the detector is $I(\tau)$.

$$E_1(t) = A_1(t)e^{i\omega_0 t} \tag{3.1}$$

$$E_2(t) = A_2(t)e^{i\omega_0 t} \tag{3.2}$$

The intensity will be proportional to the product of the sum of the fields and their conjugates:

$$I(\tau) \propto < (E_1(t-\tau) + E_2(t))(E_1(t-\tau) + E_2(t))^* > . \tag{3.3}$$

The operator $<>$ is a time average over the real time t. In the optical frequency range, ω_0 is much higher than the bandwidth of any photodetector. We have to study the average in time of the intensity.

$$I(\tau) \propto < A_1(t-\tau)^2 > + < A_2(t)^2 > + < A_1(t-\tau)^* A_2(t) > e^{i\omega_0\tau} + < A_1(t-\tau)A_2(t)^* > e^{-i\omega_0\tau} \tag{3.4}$$

The intensity has four terms. The first two are the intensities of the two branches and are just a constant value with delay. The last two are the interference term. Since they both have the same information, we can focus on studying one of them.

$$\mathcal{E}_{1,2}^+(\tau) = < A_1(t-\tau)^* A_2(t) > e^{i\omega_0\tau} \tag{3.5}$$

This function is nothing else than the cross-correlation of the two fields. Its Fourier transform is the product of the Fourier transforms of the fields.

$$\mathcal{E}_{1,2}^+(\omega) = \int_{-\infty}^{\infty} \mathcal{E}_{1,2}^+(\tau)e^{-i\omega\tau}d\tau \tag{3.6}$$

$$\mathcal{E}_{1,2}^+(\omega) = E_1^*(\omega)E_2(\omega) \tag{3.7}$$

Another way to write this is to consider the complex amplitude of the cross-correlation function:

$$\mathcal{E}_{1,2}^+(\tau) = \mathcal{A}_{1,2}^+(\tau)e^{i\omega_0\tau} \tag{3.8}$$

$$\mathcal{A}_{1,2}^+(\omega) = A_1^*(\omega)A_2(\omega). \tag{3.9}$$

These equations are independent of the light spectrum. The specificities of a white light source will be discussed in the next section.

For a perfectly balanced interferometer, without a dispersive material in one of the branches, the cross-correlation is the autocorrelation of the source. Taking the Fourier transform of the autocorrelation then gives the spectral power density of the source. The interferometer acts in this case as a spectrometer.

3.1.2 Unbalanced interferometer

Adding an element in one of the branches unbalances the interferometer, for instance a piece of glass. This adds a transfer function in one of the arms. The transfer function can be described as:

$$G(\omega) = T(\omega)e^{i\phi(\omega)}, \tag{3.10}$$

where both $T(\omega)$ and $\phi(\omega)$ are real quantities. It is split into two parts, a transmission function and an added phase that both depend on the wavelength. The first term corresponds to the imaginary part of the refractive index and the second term to its real part.

The field in the second branch is multiplied by the transmission function $T(\omega)$ and its phase is shifted. The transmission that would happen in air has to be removed and the phase term associated with the glass has to be added. For a glass of a thickness d, it gives the new field:

$$E_2(\omega) = E_1(\omega)T(\omega)e^{-id(k(\omega)-\frac{\omega}{c})}. \tag{3.11}$$

The complex valued cross-correlation becomes:

$$\mathcal{A}_{1,2}^+(\omega) = T(\omega)|E_1(\omega)|^2 e^{-id(k(\omega)-\frac{\omega}{c})}. \tag{3.12}$$

The interesting term that appears in this new cross-correlation function is the phase term $e^{-id(k(\omega)-\frac{\omega}{c})}$. $k(\omega)$ represents the dispersion characteristics of the material. Taking a Taylor expansion of k about $\omega = \omega_0$ gives a phase term of:

$$e^{-id(k(\omega)-\frac{\omega}{c})} = e^{-id(-\frac{\omega}{c}+k_0+k_1(\omega-\omega_0)+\frac{k_2}{2}(\omega-\omega_0)^2+\frac{k_3}{6}(\omega-\omega_0)^3+...)}. \tag{3.13}$$

Where:

$$k_i = \left.\frac{\partial^i k}{\partial \omega^i}\right|_{\omega_0}.$$

For instance, the first term k_0 is directly related to the value of the refractive index of the glass at the frequency ω_0:

$$k_0 = \frac{\omega_0 n(\omega_0)}{c}.$$

Taking $\Omega = \omega - \omega_0$ gives:

$$e^{-id(k(\omega)-\frac{\omega}{c})} = e^{-id(-\frac{\Omega+\omega_0}{c}+k_0+k_1\Omega+\frac{k_2}{2}\Omega^2+\frac{k_3}{6}\Omega^3+...)}. \tag{3.14}$$

Regrouping the terms by order of Ω:

$$e^{-id(k(\omega)-\frac{\omega}{c})} = e^{-id(k_0-\frac{\omega_0}{c}+(k_1-\frac{1}{c})\Omega+\frac{k_2}{2}\Omega^2+\frac{k_3}{6}\Omega^3+...)}. \tag{3.15}$$

In time domain, the consequence of this added phase is a difference in path length. Taking the Fourier transform of the added phase up to the first order highlights the delay between the two branches. Up to the first order, the relation between the two complex amplitudes in frequency is:

$$A_2(\Omega) = A_1(\Omega)e^{-id(k_0 - \frac{\omega_0}{c} + (k_1 - \frac{1}{c})\Omega)} \tag{3.16}$$

$$A_2(\Omega) = A_1(\Omega)e^{-id(k_0 - \frac{\omega_0}{c})}e^{-id\Omega(k_1 - \frac{1}{c})}. \tag{3.17}$$

When taking the inverse Fourier transform, the last term $e^{-id\Omega(k_1 - \frac{1}{c})}$ is just a delay in time:

$$A_2(t) = A_1(t - \tau)e^{-id(k_0 - \frac{\omega_0}{c})} \tag{3.18}$$

$$A_2(t) = A_1(t - \tau)e^{-\frac{id\omega_0}{c}(n(\omega_0)-1)}. \tag{3.19}$$

τ then has this expression:

$$\tau = d(k_1 - \frac{1}{c}) \tag{3.20}$$

$$\tau = d(\frac{1}{v_g} - \frac{1}{c}). \tag{3.21}$$

The effect of the first order of dispersion is indeed purely a delay of one of the arms in the time domain. The appearance of this delay is essential to the characterization of the fiber as it is directy linked to the group velocity.

3.2 Broadband source

All the previous theory was valid with any light source. This section will take a look at the theory above and the specific case of having a broadband source.

3.2.1 Coherence of a source

The first and most essential consequence of the wide bandwidth is the short coherence time.

The coherence of a source is a way to characterize the correlation of its emission at two different times, where coherence time signifies a statistical representation of the temporal difference between two points for which the correlations in the emission are lost. Coherence is divided into two categories, the spatial coherence and the temporal coherence.

Spatial coherence is the correlation of the phase in space, but not in the propagation axis, in the cross section of the beam. As an example, laser beams have a very high spatial coherence

due to the modes of the cavity. They demand specific phase conditions and make the beam spatially coherent.

The temporal coherence is the phase correlation at the same point between two different times. It is related to the bandwidth of the source. The wider the source, the shorter is its temporal coherence. A typical quantity to estimate the temporal coherence is the coherence length. It can be approximated as:

$$L_c = \sqrt{\frac{2ln2}{\pi}} \frac{\lambda^2}{n\Delta\lambda}. \tag{3.22}$$

The coherence length is a quantity that represents the distance over which the phase of the light maintains correlation, or over which it can interfere with itself.

3.2.2 Short coherence length and interferometry

In practice, the coherence length is the distance around the temporal overlap the stage can move and maintain interference on the detector. Ultrashort pulses have a broad spectrum, hence they have a short coherence length. For instance, a compressed pulse with a center wavelength of 1500 nm and a duration of 30 fs has a bandwidth of 100 nm. Its coherence length is around 15 μm.

3.3 Setup and source

3.3.1 Source options

As stated in the introduction, the only requirement for the source is the wavelength range, the two main choices are a tungsten filament source or a tunable source such as an OPA.

Thermal emitter

The first option is a thermal emitter. In our laboratory we have the source based on the hot tungsten filament, part number SLS202L [36] as provided by Thorlabs supplier. Figure 3.2 shows the spectrum of this source.

This type of source allows the complete characterization of fused silica fibers, as the transmission of fused silica drops by 3dB from the peak value at 2.3 μm.

The main issue with a filament source is the final power measured on the photodetector.
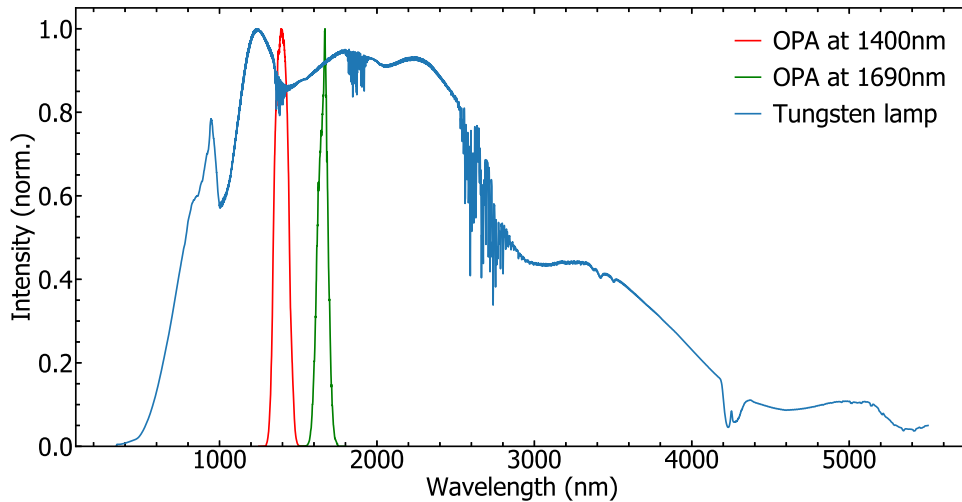
Figure 3.2 Optical spectral density of SLS202L, the power spans from 500 to 5500 nm. The data are taken from the manufacturer's website.

This comes from two characteristics of the lamp. Its spectrum is broad, so a narrow band has to be selected to have a wavelength sensitive measurement. Adding a monochromator at the end of the interferometers fulfills that purpose. The filament is not a point source, which makes the overall quality of the beam worse by degrading its spatial coherence. It can not be collimated using a parabolic mirror and focusing it gives a larger focal point than with collimated light. Focusing the beam through a 10 μm diameter pinhole creates a gaussian point source with a waist of 10 μm. Precise wavelength selection and propagation through a pinhole both lose a significant portion of the total power, degrading the SNR. Using a chopper and Lock-In Amplification would improve the SNR and allow this source to be used.

Optical Parametric Amplifier

The second option, which is the one chosen in the end is using the output of an OPA.

The OPA is an ORPHEUS-F by Light Conversion [37]. Figure 3.3 is a diagram of the OPA.

It is seeded by a pulsed light source with a wavelength of 1030 nm with pulses of 15 μJ energy and a duration of around 200 fs. It has two outputs, a signal ranging from 650 to 900 nm and an idler from 1200 to 2500 nm. Figure 3.2 shows an example of two OSA spectra with different wavelengths compared with the tungsten filament source spectrum.

The input pulse into OPA is split into two parts, the first one containing about 1% of the input energy generates a supercontinuum that is propagated in a $\chi^{(2)}$ crystal with the
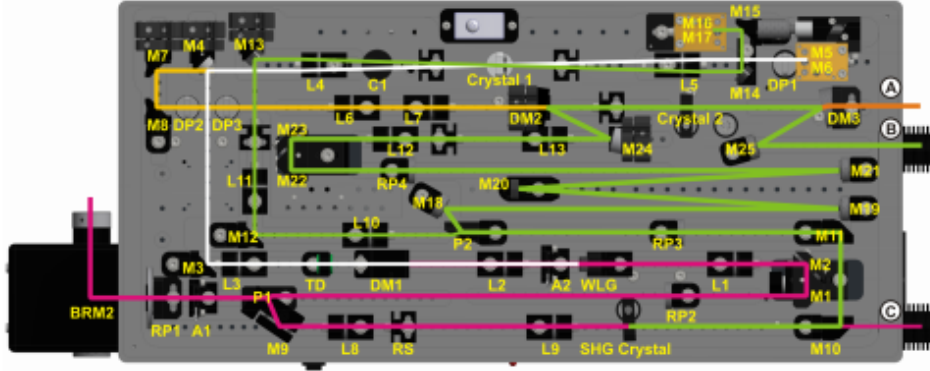
Figure 3.3 Figure taken from the ORPHEUS user manual. A are the irises, C is the compensator, DM are the dichroic mirrors, DP are the delay plates, L are the lenses, M are the mirrors, P are the polarizers, RP are the half wave plates, RS are the reflective shields, SHG is the second harmonic generation crystals and WLG is the white light generation substrate.

second one that is frequency doubled to produce the pump beam. Through parametric amplification, energy from the pump is converted to the wavelength of the signal and an idler is generated. The fundamental equation between the three components is simply the conservation of energy:

$$\hbar\omega_{pump} = \hbar\omega_{idler} + \hbar\omega_{signal}. \tag{3.23}$$

The wavelength of the converted photons depends on the phase matching in the crystal. Changing the angle of the crystal changes the generated wavelengths. An OPA is then a wavelength tunable high energy pulsed light source. Furthermore, the wavelength of the idler matches the bandwidth of the photodetector chosen. Another advantage of either one of these sources is the wide bandwidth that makes the coherence length short. This is important to find the temporal overlap efficiently.

3.3.2 Setup design

Interferometer

The setup is an unbalanced Mach-Zehnder interferometer with the fiber under characterization in one of the branches. The presence of the fiber in one of the arms unbalances the interferometer. Figure 3.4 shows a diagram of the setup.

Due to an ultrabroadband design of the dispersion characterization we minimize usage of dispersive elements in the setup. This states the requirements for thin beamsplitters. This
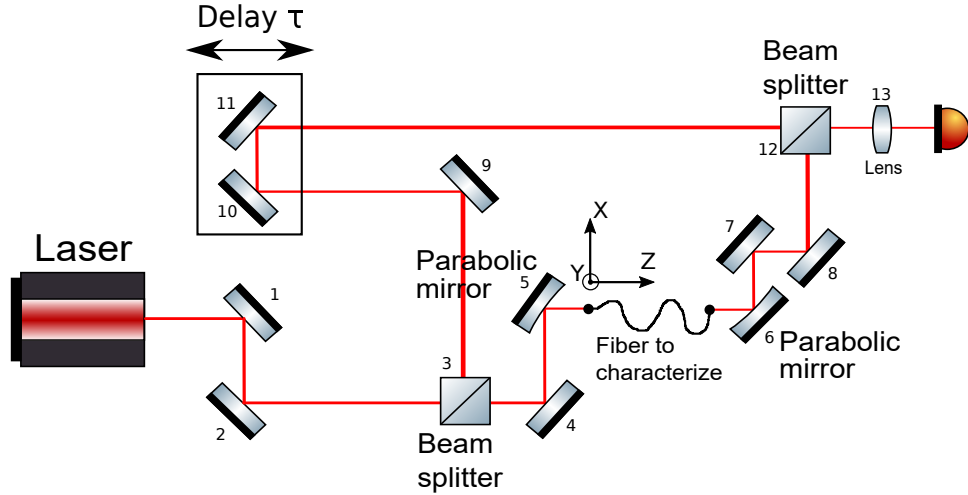
Figure 3.4 Unbalanced Mach Zehnder interferometer. Mirrors (1), (2), (4), (5), (6), (7), (8), (9), (10), (11) are flat silver coated mirrors. Beam slitters (3) and (12) are coated fused silica plates. Mirrors (5) and (6) are off axis parabolic silver coated mirrors. Finally, (13) is a fused silica lens to focus in the detector. To optimize the coupling in the fiber after mirror (5), the fiber end is mounted on a three axis translation stage and on a X and Y axis rotation stage.

is also why parabolic mirrors are used to couple in and out of the fiber instead of lenses. They are also chosen to match the NA of the fiber under characterization to maximize the coupling.

In order for the two recombined beams to interfere, they need to be spatially overlapped and their $\vec{k}$ vectors need to be collinear. The $\vec{k}$ vector of the delay line arm have to be collinear with the stage axis to keep the alignement with the stage movement. The other k vector has to be adjusted after the fiber to match.

The lower bound of the wavelength to characterize is about 1 μm. This sets the required repeatability of the stage. The repeatability of a stage is its ability to go to the same position over repeated attempts. The signal on the detector oscillates with a spatial period identical to the wavelength. Every step of a distance h of the stage increases the delay by $2h$. The Nyquist theorem states that the maximum measurable frequency is half of the sampling rate. To measure a signal with a period of 1 μm, the stage needs a repeatability of at least 250 nm. Choosing a lower one is required to increase the precision of the measurements.

The stage used is a V-508 PIMag® [38] precision linear stage. Its bidirectional repeatability is 100 nm and its travel range is 80 mm. The travel range gives flexibility in the type and length of fiber to characterize.

CHAPTER 4   MEASUREMENTS AND DISPERSION COMPUTATION

As stated in the previous chapter, the interferometer aims to measure the dispersion in optical fibers. The method to do so is to find the delay where the pulses are temporally overlapped as a function of wavelength.

4.1   Measurements

4.1.1   Zero delay search

The source used in the setup is a pulsed laser, the pulses have a duration of $T = 60$ fs. They have a spatial duration of $T \times c = 18$ μm. The temporal overlap of the pulses in the setup happens for a stage movement smaller than 10 μm. The stage has a total range of 80 mm, so finding the zero delay for any wavelength is finding a 10 μm window in a 80 mm range. Finding the zero delay requires two conditions. In order to measure an interference pattern, the $\vec{k}$ vectors have to be collinear and the beams have to be temporally overlapped. Using second harmonic generation and sum frequency generation allows to find the temporal overlap.
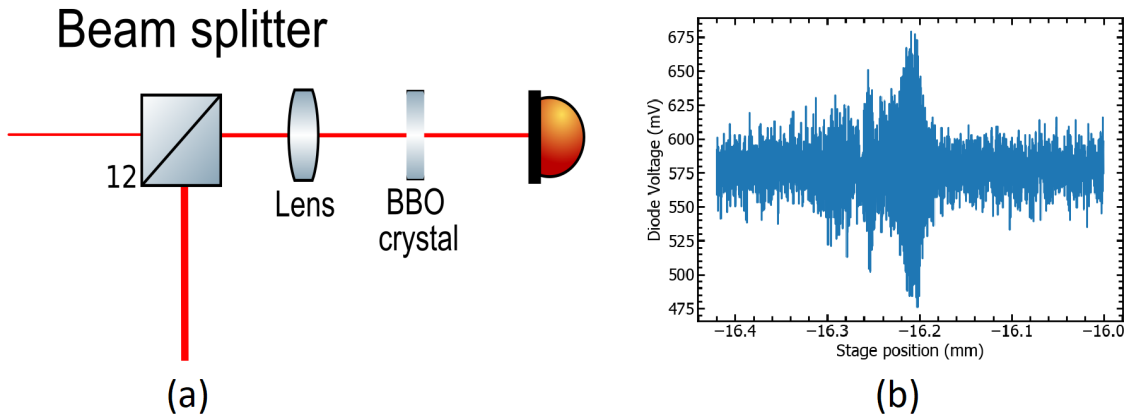
Figure 4.1 (a) Modified setup to find zero delay, a BBO crystal was added after the lens to generate frequency doubled signals. The photodetector is also switched from an InGaAs photodiode to a Si based photodiode. (b) Intensity on the photodetector as a function of the absolute stage position. The volt counts were converted to voltage in mV.

Figure 4.1(a) shows the adjustements of the setup for the zero delay search. The second harmonic of both signals are generated inside the BBO crystal. The intensity of the second

harmonic is the square of the intensity of the original signal. When the two pulses are temporally overlapped, the sum frequency of the signals is generated. The intensity of the sum frequency is the product of the intensity of each arm. So the total intensity when the pulses are overlapped is higher than when they are not. Due to the fact that $E_{SFG} = E_1 * E_2$, the contrast in the nonlinear signal should increase by a factor of 8 at the optimal temporal delay. This change is visible on a screen, so to find the zero delay, adding the BBO and manually moving the stage until the intensity increases is a viable solution. Scanning the stage around the position with the intensity spike gives a precise value of the zero delay, as Figure 4.1(b) shows. Finding one position of the zero delay is enough for all the wavelength since the variations will be very small compared to the travel range of the stage.

Once the temporal overlap is obtained with the frequency doubled signal, the adjustements to make the $\vec{k}$ vectors collinear can be done with the mirrors. The way to do so is to place the stage at the zero delay position and adjust the beam from the fiber arm to get a circular interference pattern. If the $\vec{k}$ vectors are not collinear, the interference pattern corresponds to vertical (or horizontal) fringes, the orientation depending on the misalignement between the two arms. Larger misalignment angles correspond to higher frequency of the spatial fringes on the observation screen. Even with collinear $\vec{k}$ vectors, the pattern is made of circles because the two beams are gaussian but do not have the same radius. This makes the quality of the beam collimation a critical factor, as it affects the quality of the interference pattern. A tool such as a Shack-Hartmann sensor is efficient to optimize the collimation, as Appendix A describes.

4.1.2   Signal processing

Finding the relative positions of delay where the pulses are temporally overlapped as a function of the wavelength gives access to the dispersion of the fiber. This part explains how the signals on the photodetector are processed to extract the precise position of the temporal overlap for each wavelength. Figure 4.2(a) shows an example of a scan with an aligned setup around the zero delay at a wavelength of 1560 nm.

On this measurement, the interference is clear, this is the cross-correlation of the two arms. The Fourier transform shows a single peak, as expected from the spectral profile of the OPA output (Figure 4.2(b)). The wavelength selection of the OPA serves as en effective wavelength filter. After the acquisition of the interference pattern, the next step is the processing to extract the stage position that corresponds to the temporal overlap.
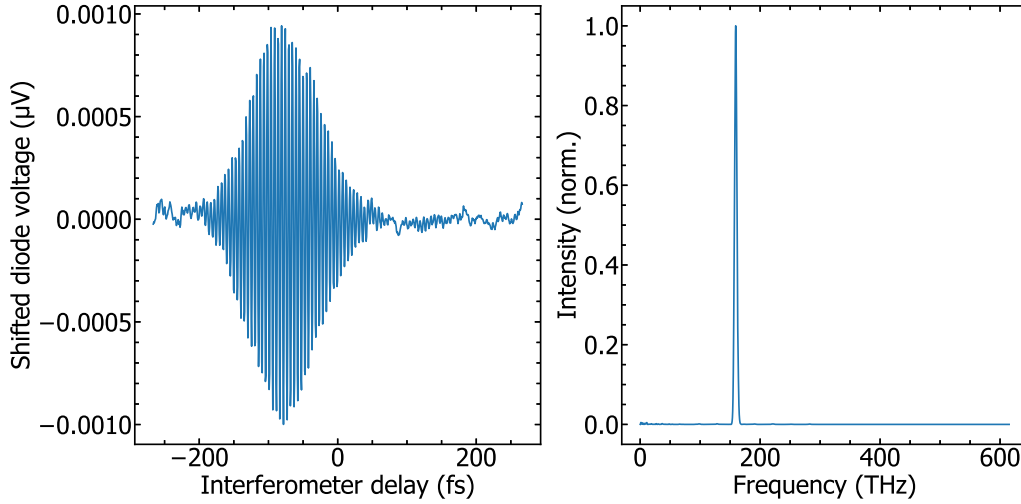
Figure 4.2 (a) Intensity on the photodetector as a function of the stage position. The averaging time per point is 50 ms. In this measurement and all the next ones, the voltage is centered around 0 because the average value is not significant. The stage position is also shifted around 0 because again, the absolute position holds no information. (b) Fourier transform of the cross-correlation. The crosscorrelation was zero padded to increase the number of points in the Fourier transform.

Hilbert Transform

The goal of this mathematical transform is to retrieve the envelope of an oscillating signal. Let's consider a signal $S(\tau)$ to analyse.

$$S(\tau) = A(\tau)\cos(\omega\tau) \tag{4.1}$$

$A(t)$ is the envelope to retrieve. The basic principle of the Hilbert transform is the following equation:

$$\cos^2(\omega\tau) + \sin^2(\omega\tau) = 1 \tag{4.2}$$

$$A^2(\tau)\cos^2(\omega\tau) + A^2(\tau)\sin^2(\omega\tau) = A^2(\tau). \tag{4.3}$$

So, to get the $A(t)$ function, we have to find the sine associated with the cos function. Applying a phase shift of $\frac{\pi}{2}$ gives the sine.

Taking the Hilbert transform of the cross-correlation and numerically filtering the high frequencies of the resulting envelope gives Figure 4.3.
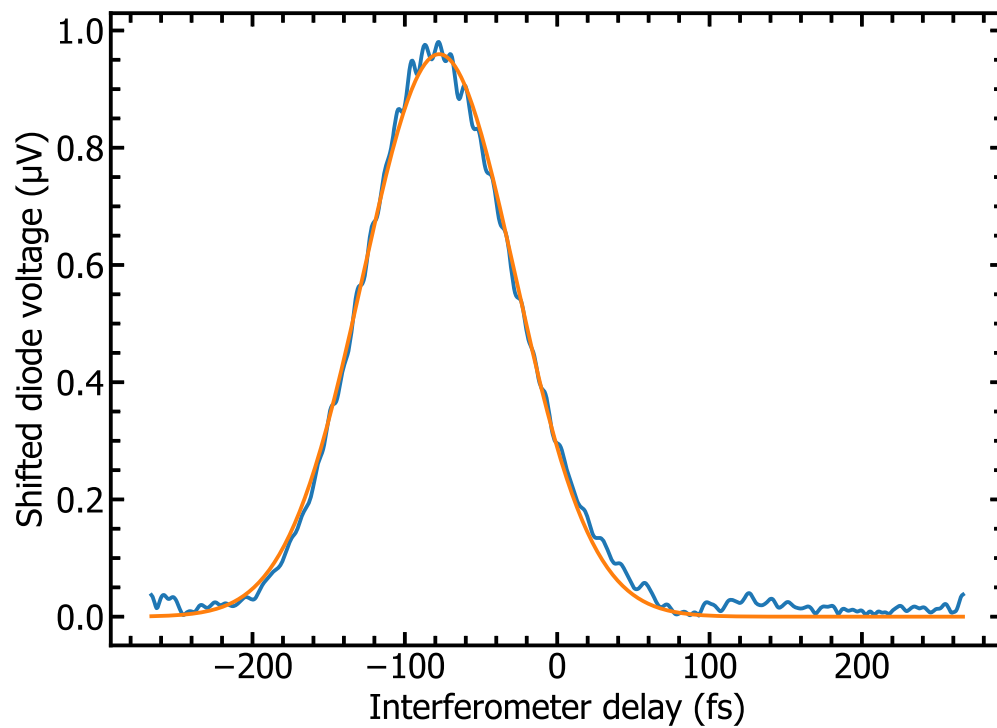
Figure 4.3 Hilbert transform of the filtered cross-correlation with a Gaussian fit. It gives the delay corresponding to the temporal overlap, in this case a relative delay of 80 fs.

4.1.3 SMF28 dispersion and comparison with manufacturer

Repeating the previous process over different wavelengths with a SMF28 fiber and plotting
the cross-correlation for different wavelenghts is shown in Figure 4.4.
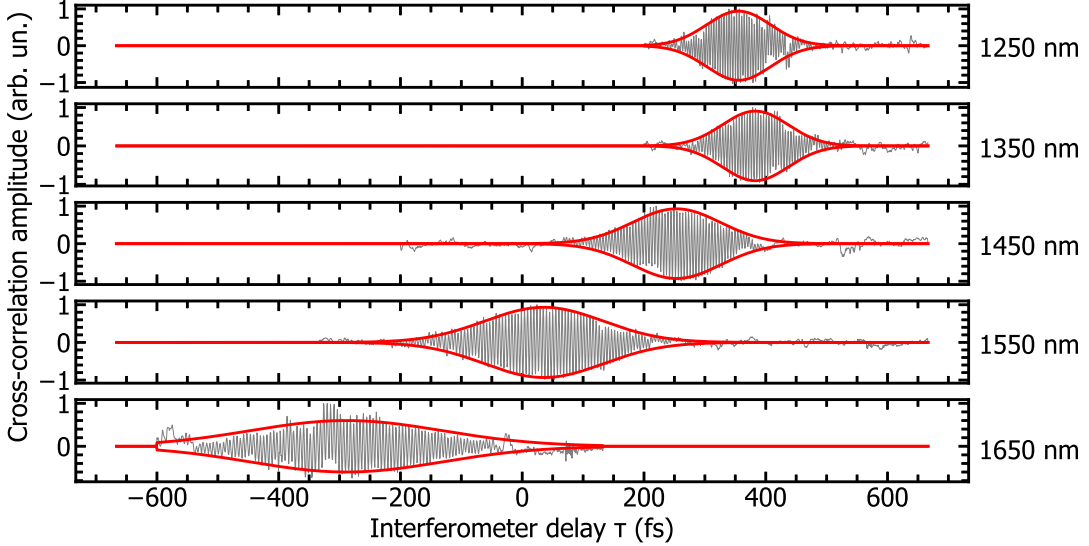
Figure 4.4 Cross-correlations at different wavelengths with Gaussian fits of the envelopes for
the SMF28. The envelopes are retrieved with a Hilbert transform. The temporal delay is
shifted of the same amount for all the wavelengths for better readability. The y axes are the
intensity on the photodetector as on the previous cross-correlations.

The overlap delay τ_0 can then be obtained as a function of wavelength. Figure 4.5 shows
this. The next step is to take the plot of the delay and extract the dispersion.

Dispersion extraction

The ovrelap delay $\tau_0(\omega)$ follows equation (4.4) that allows to extract the dispersion:

$$\Delta\tau_0(\omega) = L_f \Delta(\frac{1}{v_g}), \tag{4.4}$$

where L_f is the length of the fiber. All the quantities are defined relative to an absolute
delay. Luckily, what we are interested in is not the group velocity, but the variation of the
group velocity with wavelength, the group velocity dispersion given by:
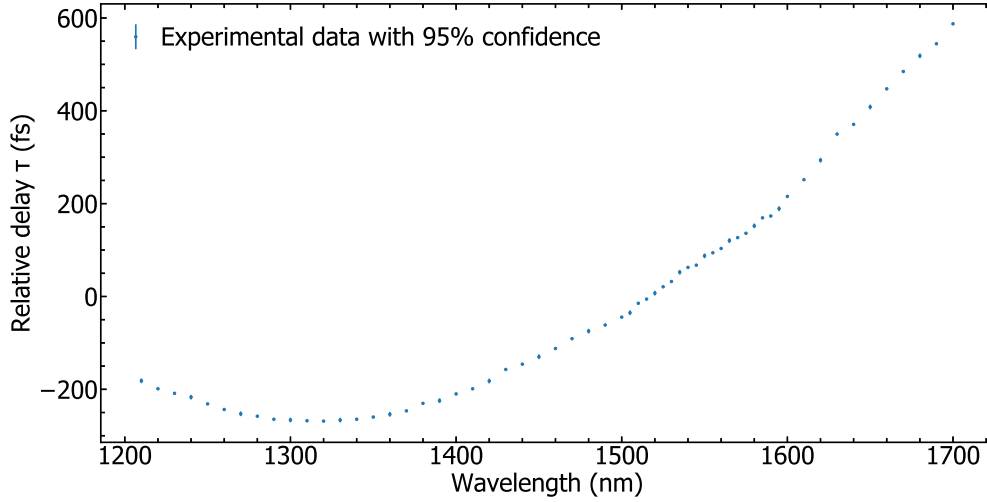
Figure 4.5 Zero delay τ as a function of wavelength. The central positions of the Gaussians fit are taken and plotted as a function of the input wavelength. The delay was shifted again as the important quantity is the relative delay.

$$GVD = \frac{\partial^2 k}{\partial \omega^2} \tag{4.5}$$

$$GVD = \frac{\partial}{\partial \omega} \frac{1}{v_g}. \tag{4.6}$$

Taking the derivative of equation (4.4) gives directly the GVD:

$$\frac{\partial}{\partial \omega} \Delta \tau(\omega) = = L_f \times GVD \tag{4.7}$$

$$GVD = \frac{\partial}{\partial \omega} \frac{\Delta \tau(\omega)}{L_f}. \tag{4.8}$$

Instead of taking a numerical derivative of the delay, a polynomial function of the following form: $F(\tau) = a + b\tau + c\tau^2 + d\tau^3$ is fitted to the delay curve 4.6. The choice of third degree is motivated by the evolution of the quality factor of the fit as detailed further in section (4.2.3).

Taking the derivative of the delay gives the dispersion coefficient of the fiber shown in Figure 4.7. The dispersion coefficient is the typical quantity used to describe dispersion in optical
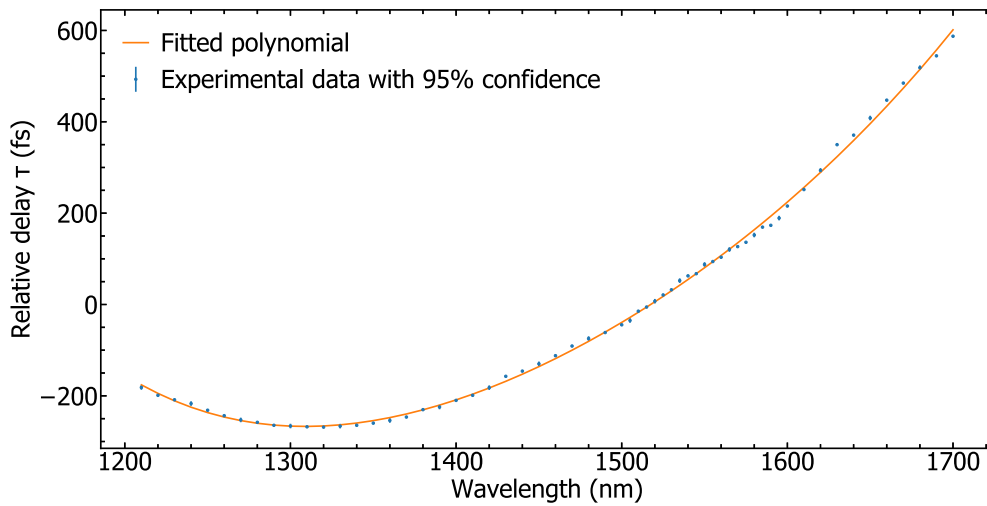
Figure 4.6 Polynomial fit of degree three of the measured delay.

fibers.
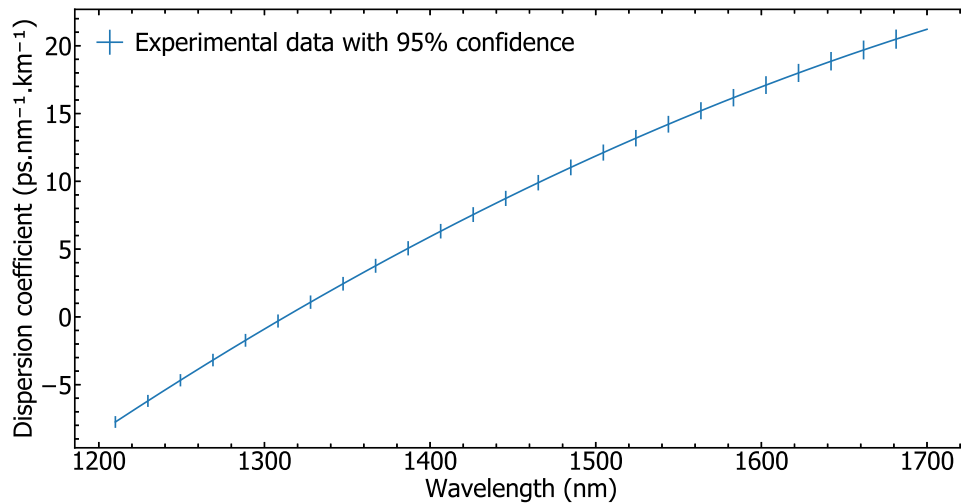
Figure 4.7 Dispersion coefficient of SMF28 with a fiber length $L_f = 18.8$ cm. It is the derivative of the delay as a function of the wavelength. The dispersion is given by the dispersion coefficient D more common than GVD for optical fibers. The uncertainty is obtained by taking the all the polynomial functions that fit within the errorbars.

$$D = \frac{\partial}{\partial \lambda} \frac{1}{v_g} \tag{4.9}$$

$$D = -\frac{2\pi c}{\lambda^2}.\text{GVD} \tag{4.10}$$

The dispersion of SMF28 is well known, the main manufacturer of SMF28 Corning® gives their dispersion equation and the parameters for SMF28:

$$D(\lambda) = \frac{S_0}{4}(\lambda - \frac{\lambda_0^4}{\lambda^3}) \tag{4.11}$$

$$S_0 < 0.092 \text{ ps.nm}^{-2} \tag{4.12}$$

$$\lambda_0 = 1311 \text{ nm.} \tag{4.13}$$

The S_0 parameter is the slope of the dispersion coefficient at the zero dispersion wavelength λ_0. Corning® specifies a worst case scenario for the slope. Taking $S_0 = 0.087$ ps.nm^{-2}, $\lambda_0 = 1312$ nm and plotting both the dispersion equation and the measurement gives Figure 4.8.
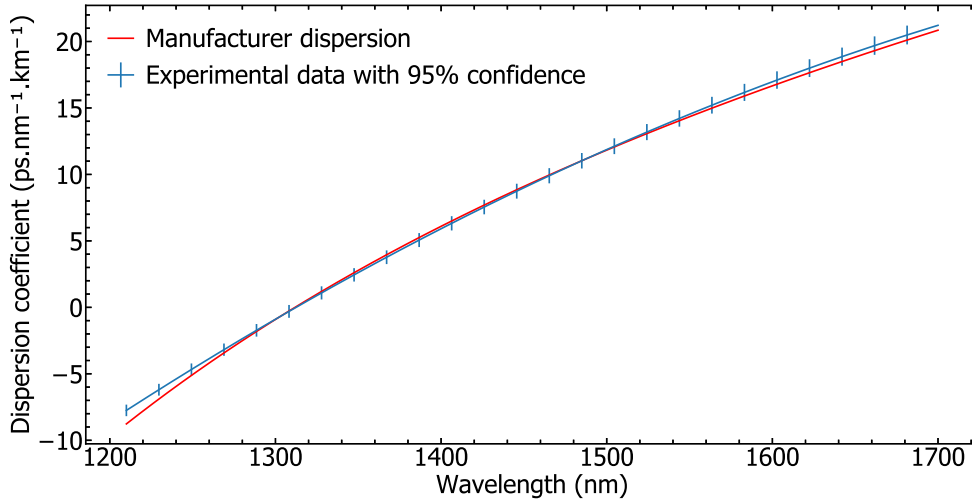
Figure 4.8 Comparison between the measured dispersion and the dispersion equation given by Corning. Both results are based on experimental input.

There is a clear match between the manufacturer's data and the data I measured. The manufacturer's curve is within the errorbars. Furthermore, the region of interest for Corning®

is the wavelength between the ZDW of SMF28 (1310 nm) and the telecommunication region (1500-1600 nm). This is the region where the agreement between the two set of data is the strongest, confirming the accuracy of the interferometer.

4.1.4   Highly nonlinear fiber

After the characterization of SMF28, the next step is to characterize a fiber with an unknown dispersion. Here I present the results of a specialty dispersion-shifted fiber produced in 2004 by the group of Prof. Younnès Messadeq at the Univ. Laval (fiber 2004C7). It is a highly nonlinear fiber with a smaller core than SMF28. The typical core diameter for a SMF28 fiber is around 8 μm and the core of the HNF is 3.2 μm.

The same process was applied to find the dispersion of this fiber. Figure 4.9 shows different cross-correlations for the HNF.
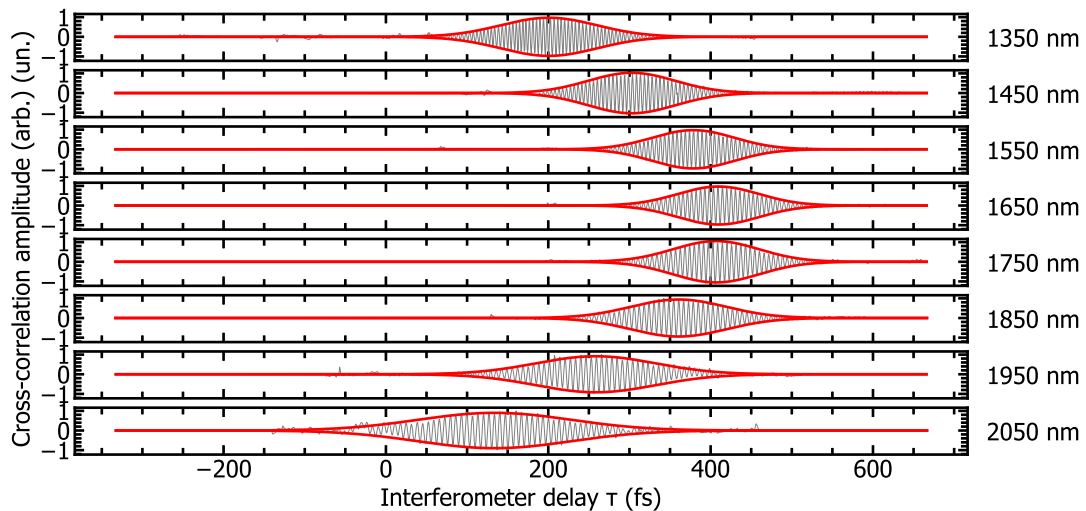
Figure 4.9 Cross-correlations at different wavelengths with Gaussian fits of the Hilbert transforms of the envelopes for the HNF. The delay is shifted for more visibility. The shift is identical at all the wavelength to show the relative position of the temporal overlap delay. The y axis are the intensity on the photodetector as on the previous cross-correlations.

In this case, there is no manufacturer curve available for comparison. The first thing to notice is the shift in the zero dispersion wavelength. In the case of SMF28, the zero dispersion wavelength is around 1300 nm whereas for this fiber, it is around 1670 nm.
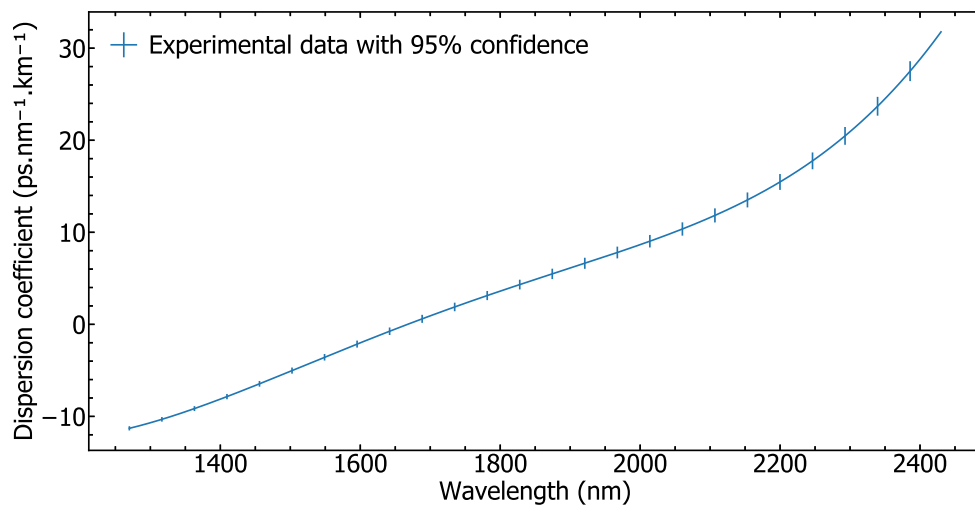
Figure 4.10 Dispersion coefficient of the HNF with a fiber length $L_f = 14.4$ cm.

4.2   Signal uncertainty

4.2.1   Noise sources

The main sources of noise in the setup are the optical elements, and more particularly the beam splitter holder that are 3D printed in plastic. They induce vibrations that perturb the signal. The vibrations come from the air current fluctuations and from structural vibrations in the building.

The choice of the measurements devices is the best way to improve the SNR in this type of setup. The detector is an InGaAs photodiode with a noise equivalent power of $1.5 \text{ pW.Hz}^{\frac{1}{2}}$. This type of detector typically has a pink noise in $\frac{1}{f}$. The noise measurement was done with the stage fixed in the middle of the interference fringes, then the Fourier transform of the time-domain evolution of the signal is taken in Figure 4.11.
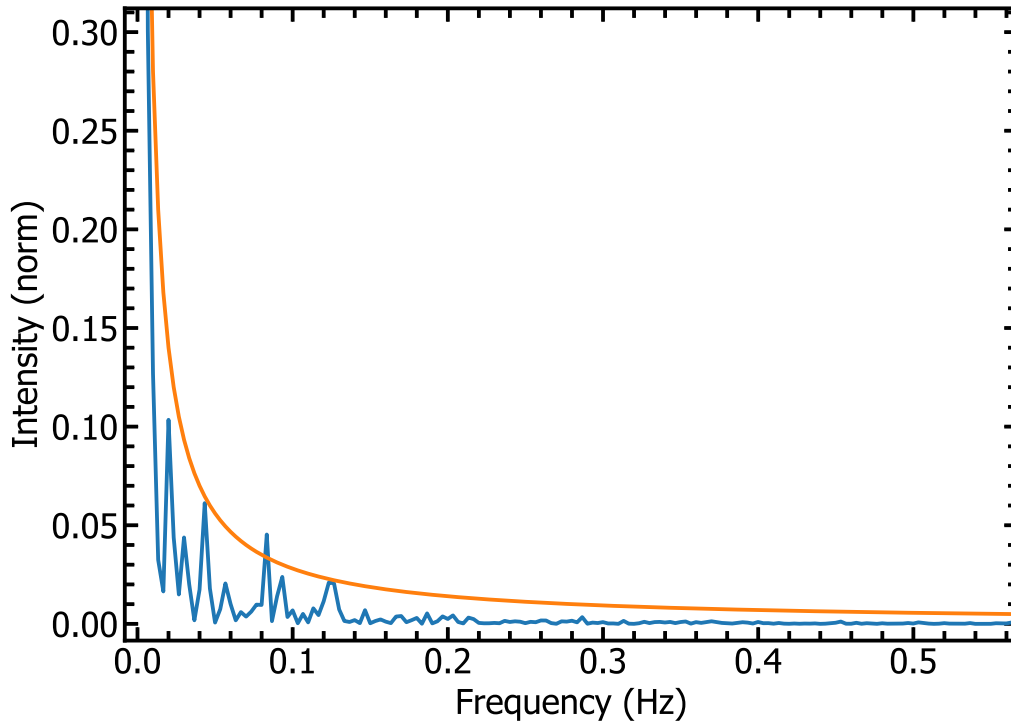
Figure 4.11 Fourier transform of the diode signal with a 1/f curve. The signal was acquired with the OPA as an input with no movement of the delay stage. The peaks in the Fourier transform correspond to low frequency vibrations that are not filtered by the optical table.

As expected, the lower frequencies exhibit a pink noise.

4.2.2 SNR optimization

A box made of coroplast put on top of the setup cuts the majority of the air and limits the vibrations of the optical elements. A better solution would be a more sophisticated box with metal panels and holes for the light inputs and outputs.

Measurement techniques

There is not much choice when it comes to the detector. It has to cover the whole range of wavelength to characterize and have the lowest available noise equivalent power. A photodiode is the only realistic solution.

The first Digital to Analog Converter used was a Redcard acquisition card with a 100 Hz bandwidth. As the source is pulsed with a repetition rate of 1 MHz, an electronic low pass filter was added to integrate the signal and match the bandwidth of the card. However, it loses all the information outside of the detector bandwidth. Additionaly, the card exhibits readout noise.

Using this kind of setup with the acquisition card gives the kind of trace given in Figure 4.1(b).

The SNR is about 4 in this case, for an averaging time per point of 100 ms. Since the input is pulsed light with a fixed repetition rate, a Boxcar can improve it.

Boxcar

A boxcar is a software signal processing tool, which selects a part of a periodic signal. In this case, the boxcar gate was numerically applied by the Zurich Instruments LIA. It applies a periodic temporal gate. Figure 4.12 shows a theoretical temporal signal with the boxcar gate.

As predicted, using a boxcar increases signal to noise, as the comparison between Figures 4.1(b) and 4.2(a) shows. Figure 4.2(a) has a SNR of about 15 with a shorter averaging time per point of 50 ms.

4.2.3 Error in the dispersion curve

The goal of this section is to estimate and plot this uncertainty in all the steps of the dispersion characterization.

Doing five identical stage scans for each wavelength and extracting the temporal overlap
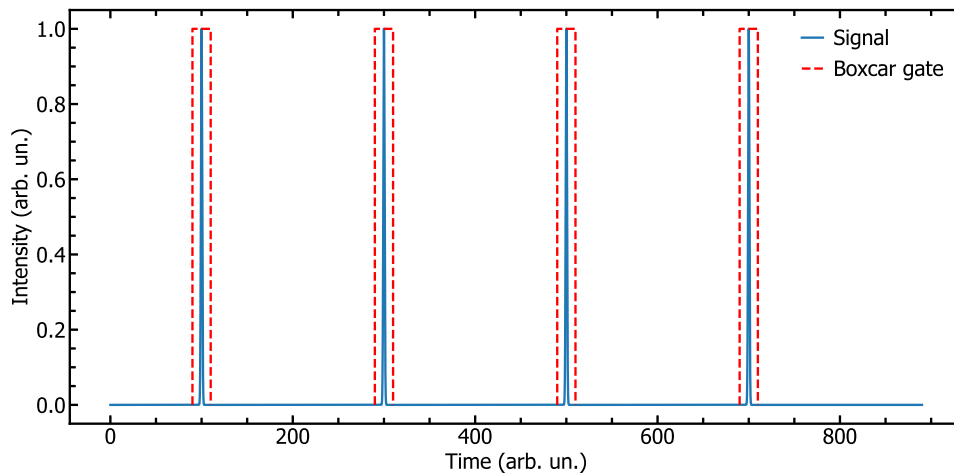
Figure 4.12 A sketch of the periodic signal arising from a train of pulses with a boxcar gate applied with a matching period.

position for the HNF and taking a 95% confidence interval gives the result represented in Figure 4.13.
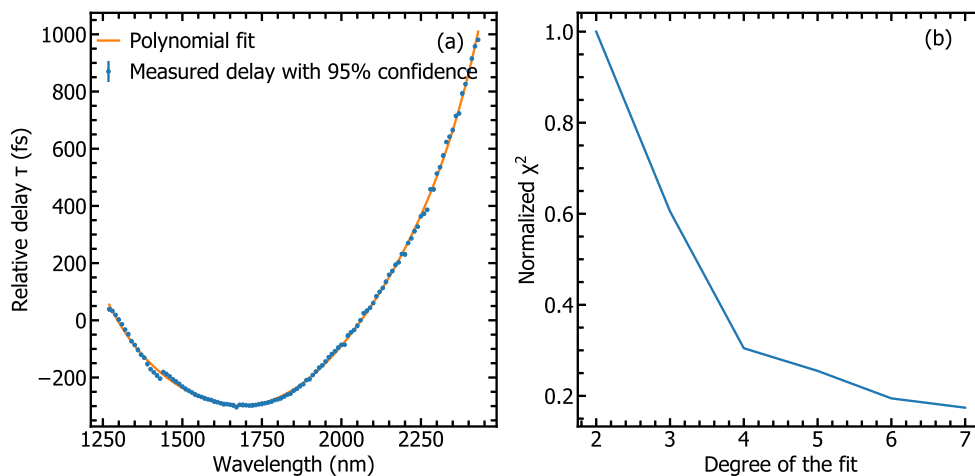
Figure 4.13 (a) 95% confidence interval on the zero delay measurement for the 2004C7 fiber and a degree six polynomial fit. (b) Value of χ^2 as a function of the polynomial degree. Degree 6 reaches a plateau in χ^2 value. Further increasing degree would insignificantly decrease error, but would not necessarily add information.

Obtaining the dispersion function from the delay comes back to taking a first derivative of the polynomial fit of the measured wavelength-dependent delay data. The quality of the fit

is defined by the χ^2 factor, it quantifies the difference between the signal and the fit. Naming the signal to fit S and the fitting function F and indexing the points gives the following expression to χ^2.

$$\chi^2 = \sum_i \frac{(F_i - S_i)^2}{F_i} \tag{4.14}$$

The reason behind chosing a degree six fit is the tendency of variation for the χ^2 factor as a function of the polynomial degree. The normalized parameter is equal to 1 for a degree 3, 0.27 for a degree 5, 0.21 for a degree 6 and 0.2 for a degree 7. Increasing the degree to 6 significantly reduces the error factor, compared to going to degree 7.

Incorporating the error bars in the polynomial fit gives uncertainty on the coefficients. This gives the uncertainty curves of the Figures 4.10 and 4.7.

The last aspect of this setup that can impact the quality of the signal are nonlinear effects in the fiber.

4.2.4   Nonlinear effects

The next chapter studies the supercontinuum generation in the characterized fiber. However, when these effects happen during the measurement, they only decrease the signal.

Since the source is pulsed and high energy, nonlinear effects can occur in the fiber.

SPM and Kerr effect

The origin of self phase modulation is third order nonlinearities, more precisely optical Kerr effect, where the refractive index acquires intensity-dependent contributions:

$$n(I) = n_0 + n_2 I, \tag{4.15}$$

where n_2 is a coefficient intrisic to the material that corresponds to the amount of refractive index change with intensity. As a consequence, when propagating light with high enough intensity to where the change in refractive index is significant, the input broadens in frequency.

Without taking any precaution to get rid of these effects, the crosscorrelation signal with appreciable SPM action is shown in Figure 4.14(a). Its corresponding Fourier transform is shown in Figure 4.14(b). While the Fourier transform of cross-correlation with nonlinear optical contributions does not directly correspond to the spectral density of the source, the spectral shape exhibits well-defined lobes where production of new frequencies, characteristic of SPM processes, is evident. Correspondingly in the time domain, arrival times of the main spectral components and newly generated wings are different due to the additional and nonlinear dispersion introduced through time-modulated refractive index (Fourier transform of Eq 4.15).

Despite having an oscillating signal at some carrier frequency, we do not see any clear bell-shaped envelope on Figure 4.14(a). It shows the typical behaviour of SPM with a spectrum with secondary maximums around the main peak. Because of the spectral broadening, most of the power of the fundamental is transfered around it. This results in lower power in the cross-correlation, as it is the product of the spectra of both branches. To avoid detrimental nonlinearities in the signal, all the successful measurements were taken with a neutral density filter in front of the setup that filtered with a factor of 10 000. This is one of the main reasons why the use of a boxcar was mandatory to get a SNR that made the signal exploitable.
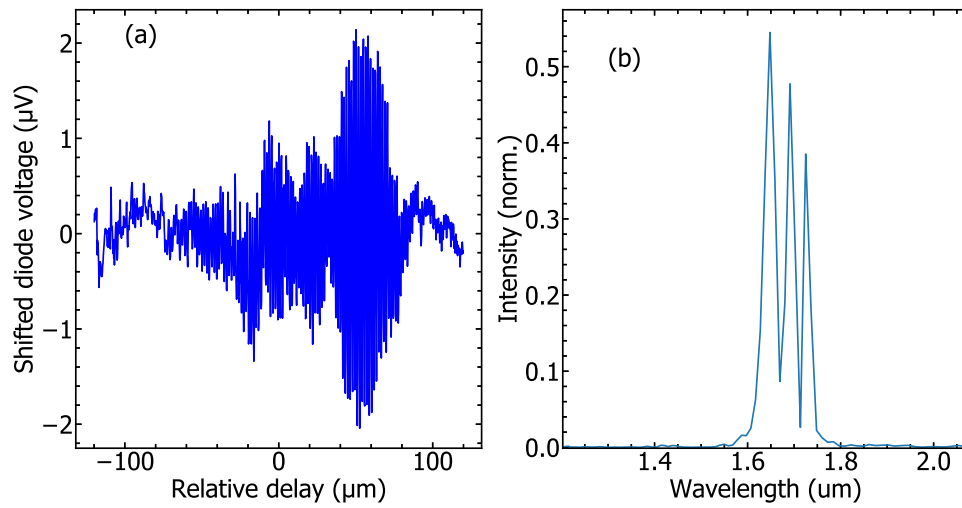
Figure 4.14 (a) Autocorrelation with the full power of the OPA injected in the setup. This was taken with SMF28. (b) Fourier transform of (a). It is no longer a single peak but has secondary peaks around the main one.

4.2.5   Other possible applications for the setup

Nonlinear coefficient

Having the presence of the nonlinear effects of the fiber opens up for a alternative use of the characterization setup. It could indeed be used to find the n_2 parameter and its dispersion in optical fibers. One way to do so would be to take a look at the interference pattern with varying the intensity of the light input in the setup.

Higher order modes

For wavelenghts shorter than the single-mode waveguide cutoff of the fiber (e. g. in SMF28 it corresponds to 1260 nm), the propagation condition is supported for higher order spatial modes. Exemplary Hilbert transform of the crosscorrelation signal at an input wavelength of 1200 nm is shown in Figure 4.15. The input is sufficiently attenuated such that no nonlinear processes, such as SPM, take place. In addition to the main peak situated at a relative delay of approximately -250 fs, there appear two new peaks centered at -30 and 200 fs relative delays, respectively. We attribute the main peak corresponding to the fundamental mode of the fiber, while the other two are evidence of the higher-order guided modes. The picture was corroborated by the spatial mode patterns observed on the screen after the fiber. While this was not the focus on this study, multimodal structural dispersion can also be characterized in our setup, perhaps with additional input from spatial imaging to correlate spatial and spectral mode decomposition.
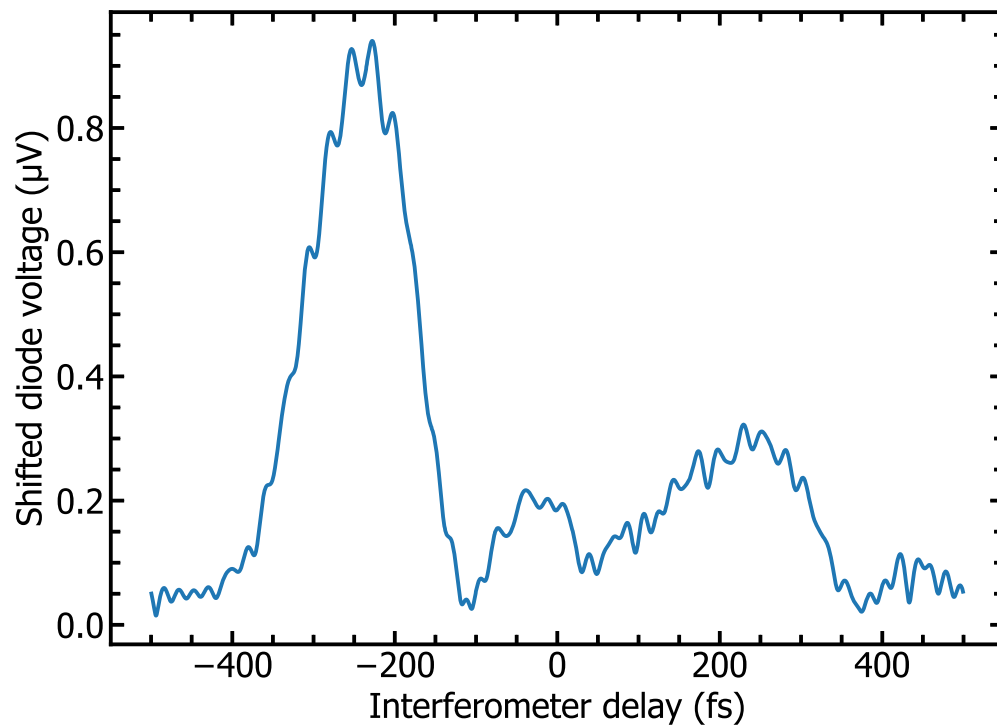
Figure 4.15 Hilbert transform of a crosscorrelation with SMF28 with an input wavelength of 1200 nm. The first peak corresponds to the fundamental mode, the later peaks are due to higher order modes.

CHAPTER 5   SUPERCONTINUUM GENERATION IN HIGHLY NONLINEAR FIBERS AND ITS SIMULATION

The main objective of this section is to maximize the spectral broadening of an ultrashort pulse using nonlinear effects, more specifically supercontinuum generation. The final desired result is to obtain a spectral bandwidth broad enough to support single cycle pulse generation.

5.1   Simulation of pulse broadening in highly nonlinear fiber

All the theory explained in this part is based on the second chapter of "Nonlinear Fiber Optics" textbook by G. Agrawal [17].

This section summarizes the way to simulate the propagation of a short pulse in an optical fiber. The goal is to combine the nonlinear effects and the dispersion of the fiber. The challenge is that the nonlinearities are easier to process in the time domain while the dispersion is easier to process in the frequency domain.

5.1.1   Propagation equation

The starting equation of the simulation is a simple wave equation expressed with the electric field and the polarization:

$$\nabla^2 \mathbf{E} = -\frac{1}{c^2}\frac{\partial^2 \mathbf{E}}{\partial t^2} - \mu_0 \frac{\partial^2 \mathbf{P}}{\partial t^2}. \tag{5.1}$$

The nonlinear effects appear in the polarization vector. It can be split into two parts, the linear part that is proportional to the electric field and the nonlinear part that is not:

$$\mathbf{P}(r,t) = \mathbf{P}_L(r,t) + \mathbf{P}_{NL}(r,t). \tag{5.2}$$

Incorporating this separation in the wave equation gives:

$$\nabla^2 \mathbf{E} - \frac{1}{c^2}\frac{\partial^2 \mathbf{E}}{\partial t^2} = \mu_0 \frac{\partial^2 \mathbf{P}_L}{\partial t^2} + \mu_0 \frac{\partial^2 \mathbf{P}_{NL}}{\partial t^2}. \tag{5.3}$$

To further simplify and process this equation, the envelope and the oscillating parts of the fields involved are defined:

$$\mathbf{E}(r,t) = \frac{1}{2}\hat{x}[E(r,t)exp(-i\omega_0 t) + c.c.] \tag{5.4}$$

$$\mathbf{P}_L(r,t) = \frac{1}{2}\hat{x}[P_L(r,t)exp(-i\omega_0 t) + c.c.] \tag{5.5}$$

$$\mathbf{P}_{NL}(r,t) = \frac{1}{2}\hat{x}[P_{NL}(r,t)exp(-i\omega_0 t) + c.c.], \tag{5.6}$$

where $\hat{x}$ is the unit vector in the same direction that the polarization, and ω_0 is the center frequency of the propagating pulse. In addition, the Fourier transforms of the fields are defined as the next equation shows:

$$\tilde{E}(r,\omega - \omega_0) = \int_{-\infty}^{\infty} E(r,t)exp(i(\omega - \omega_0)t)dt. \tag{5.7}$$

Taking the wave equation to the Fourier domain shows that the electric fields follows the Helmholtz equation:

$$\nabla^2 \tilde{E} + \varepsilon(\omega)k_0^2 \tilde{E} = 0, \tag{5.8}$$

with $k_0 = \frac{\omega}{c}$. ε is the dielectric function and can also be split into the linear and the nonlinear parts.

$$\varepsilon(\omega) = 1 + \chi^{(1)}(\omega) + \varepsilon_{NL}(\omega) \tag{5.9}$$

The nonlinear part of the dielectric function affects the refractive index and the absorption coefficient α of the material and adds a dependence with intensity:

$$n = n_0 + n_2|E|^2 \tag{5.10}$$

$$\alpha = \alpha_0 + \alpha_2|E|^2. \tag{5.11}$$

The loss term α_2 is connected to two photon absorption and will be ignored as it is negligible in silica fibers.

Separating the variables in the field allows to solve the wave equation in the frequency domain:

$$\tilde{E}(r, \omega - \omega_0) = F(x, y)\tilde{A}(z, \omega - \omega_0)exp(i\beta_0 z). \tag{5.12}$$

The F function is the distribution of the field in the core of the fiber in a section plane, β_0 is the propagation constant and the $\tilde{A}$ function is the Fourier transform of the envelope of the pulse slowly varying along the z axis. This is the function of interest in our case. Solving equation (5.8) gives two separate equations for $\tilde{A}$ and F:

$$\frac{\partial^2 F}{\partial x^2} + \frac{\partial^2 F}{\partial y^2} + (\varepsilon(\omega)k_0^2 - \tilde{\beta}^2)F = 0 \tag{5.13}$$

$$2i\beta_0 \frac{\partial \tilde{A}}{\partial z} + (\tilde{\beta}^2 - \beta_0^2)\tilde{A} = 0. \tag{5.14}$$

Equation (5.13) can be solved to find the propagation constant $\tilde{\beta}$ with perturbation theory. Naming the first order perturbation $\Delta\beta$ gives the following equation for $\tilde{A}$:

$$\frac{\partial \tilde{A}}{\partial z} = i(\beta(\omega) + \Delta\beta(\omega) - \beta_0)\tilde{A}. \tag{5.15}$$

The meaning of this equation is fairly simple to understand, the envelope experiences a phase shift that is frequency dependent and one that is intensity dependent.

Since the $\beta(\omega)$ is usually not an analytical function, a Taylor expansion is often used to describe it:

$$\beta(\omega) = \beta_0 + (\omega - \omega_0)\beta_1 + \frac{1}{2}(\omega - \omega_0)^2\beta_2 + \frac{1}{6}(\omega - \omega_0)^3\beta_2 + ... \tag{5.16}$$

Going back to the time domain gives this equation for the envelope:

$$\frac{\partial A}{\partial z} + \beta_1 \frac{\partial A}{\partial t} + \frac{i\beta_2}{2} \frac{\partial^2 A}{\partial t^2} = i\Delta\beta_0 A. \tag{5.17}$$

$\Delta\beta_0$ is a term that regroups the effects of the nonlinearities and the losses in the fiber. Expressing these effects individually gives:

$$\frac{\partial A}{\partial z} + \beta_1 \frac{\partial A}{\partial t} + \frac{i\beta_2}{2} \frac{\partial^2 A}{\partial t^2} + \frac{\alpha}{2} A = i\gamma(\omega_0)|A|^2 A, \tag{5.18}$$

where:

$$\gamma(\omega_0) = \frac{n_2(\omega_0)\omega_0}{cA_{\text{eff}}}. \tag{5.19}$$

A_{eff} is the effective area of the fundamental mode of the fiber.

In the previous propagation equation (5.18), higher order nonlinearities were neglected, more particularly the Raman effect. It can be modeled by this response function:

$$R(t) = (1 - f_R)\delta(t - t_e) + f_R h_R(t), \tag{5.20}$$

where t_e is a parameter that accounts for the delay in the system, f_R and h_R characterize the Raman response of the material. A standard form of the Raman response function is:

$$h_R(t) = \frac{\tau_1^2 + \tau_2^2}{\tau_1 \tau_2^2} exp(\frac{-t}{\tau_2})sin(\frac{t}{\tau_1}), \text{ for } t > 0 \tag{5.21}$$

The last parameter to introduce is the first moment of the nonlinear response function:

$$T_R = \int_0^{+\infty} tR(t)dt. \tag{5.22}$$

Adding these effects to the differential equation of the envelope gives a new equation:

$$\frac{\partial A}{\partial z} + \frac{\alpha}{2}A + \frac{i\beta_2}{2}\frac{\partial^2 A}{\partial T^2} - \frac{\beta_3}{6}\frac{\partial^3 A}{\partial T^3} = i\gamma\left(|A|^2 A + \frac{i}{\omega_0}\frac{\partial}{\partial T}(|A|^2 A) - T_R A\frac{\partial |A|^2}{\partial T}\right). \tag{5.23}$$

T is simply the time variable but shifted to follow the pulse propagation:

$$T = t - \frac{z}{v_g}. \tag{5.24}$$

Once again here, two parts of the equation appear, the left side is the dispersion whereas the right part is the nonlinear effects.

5.1.2 Numerical consideration

Equation (5.23) is the equation that describes the evolution of the pulse envelope along the fiber. However, the analytical solution, if it exists, is unknown. An efficient way to approach this equation is to attempt to solve it numerically. This section details the numerical process behind the solving of this equation.

The difficulty of the solving comes from the duality of the effects to consider. On the one hand, the dispersion affects the spectral phase of the pulse, on the other hand the nonlinear effects modify the amplitude of the spectrum. The equation can be rewritten with two different operators to separate dispersion and nonlinearities:

$$\frac{\partial A}{\partial z} = (\hat{D} + \hat{N})A, \tag{5.25}$$

$$\hat{D} = -\frac{i\beta_2}{2}\frac{\partial^2 A}{\partial T^2} + \frac{\beta_3}{6}\frac{\partial^3 A}{\partial T^3} - \frac{\alpha}{2}A, \tag{5.26}$$

$$\hat{N} = i\gamma\left(|A|^2 A + \frac{i}{\omega_0}\frac{\partial}{\partial T}(|A|^2 A) - T_R A\frac{\partial |A|^2}{\partial T}\right). \tag{5.27}$$

In reality, these effects happen at the same time along the pulse propagation. In order to be able to compute them, they have to be treated separately. The method that is going to be used is the *split-step Fourier method*.

The easiest way to compute the dispersion is to work in the frequency domain and to simply add a phase shift to the pulse. For the nonlinear effects, the best way is to apply them in the time domain. The split-step Fourier method is a way to compute where the dispersion

is applied in the frequency domain in a small portion of the fiber, then the inverse Fourier transform is taken to apply nonlinearities.

From equation (5.25), the simple process to progress a step of length h is given by:

$$A(z + h, T) = exp(h(\hat{D} + \hat{N}))A(z, T). \tag{5.28}$$

The approximation to compute is the separation of the operators. It assumes that on distances small enough dispersion and nonlinearities act independently:

$$A(z + h, T) \approx exp(h\hat{D})exp(h\hat{N})A(z, T). \tag{5.29}$$

The final step to improve the accuracy of this method is to take the integral of the $\hat{N}$ operator over a segment of length h and to apply a half step dispersion before and a half step after.

$$A(z + h, T) \approx exp(\frac{h}{2}\hat{D})exp(\int_z^{z+h} \hat{N}(z')dz')exp(\frac{h}{2}\hat{D})A(z, T) \tag{5.30}$$

In practice, $\hat{N}$ is unknown in $(z + h)$, so the calculation will be an iterative process inside a step h.

5.1.3 Results of the simulation

Having characterized the dispersion of a highly nonlinear fiber allows to simulate the propagation of an ultrashort pulse in said fiber. The following simulations were computed using a python software called PyNLO [39]. The objective of this first simulation is to find the optimal input energy and fiber length to optimize the bandwidth at the output of the fiber. The experimental is going to be the OPA attenuated by a factor of 10. The resulting energy is of the order of a few nJ. Figure 5.1 shows a surface plot of the power spectral density using a logarithmic scale after propagating a pulse with a varying energy in 2 cm of highly nonlinear fiber. The best results are generally obtained with small lengths of fiber, in this case, 2 cm is the lower limit due to the experimental setup.

For low input pulse energies, the spectral broadening is only caused by SPM. When the input energy reaches about 6 nJ, there is a splitting of the pulse energy to a soliton in the negative
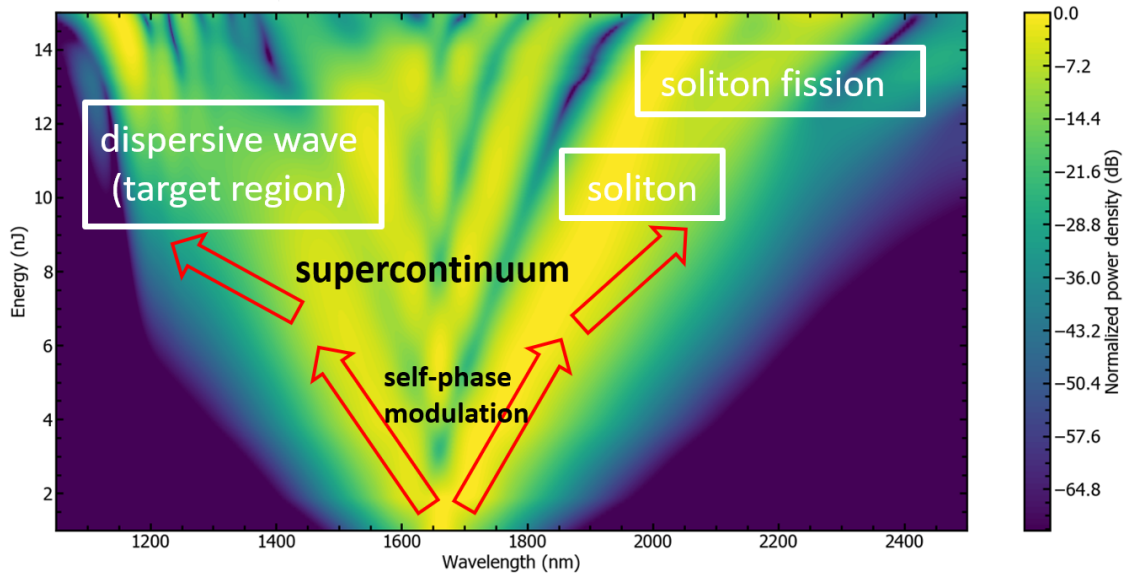
Figure 5.1 Surface plot of the power spectral density at the output of 2 cm of 2004C7 as a function of input energy. The input is a theoretical Gaussian pulse with a FWHM duration of 60 fs and a central wavelength of 1660 nm.

GVD regime (long wavelength components from the zero-dispersion wavelength) as well as the dispersive wave, appearing at shorter wavelengths components, where GVD is positive. The energy of interest is the energy that generates the broadest dispersive wave with a flat spectrum. At energies higher than 12 nJ, the repartition of energy becomes irregular. Figure 5.2 shows the particular spectra with 12 and 14 nJ inputs.

As expected with the surface plot, an input energy gives a more uniform repartition of energy in the dispersive wave, making it an ideal candidate for experimental supercontinuum generation.

5.2 Comparison with the experiments

The next goal is to use the simulation tool to reproduce results acquired in the laboratory.

5.2.1 Laboratory setup

The generation setup takes the output of the OPA and couples it in 2 cm of a Highly Nonlinear Fiber. Figure 5.3 shows a diagram of the setup.

The main objective of this setup is to generate supercontinuum and to optimize it. The source is the same as the one used for the characterization of dispersion, namely, a pulsed
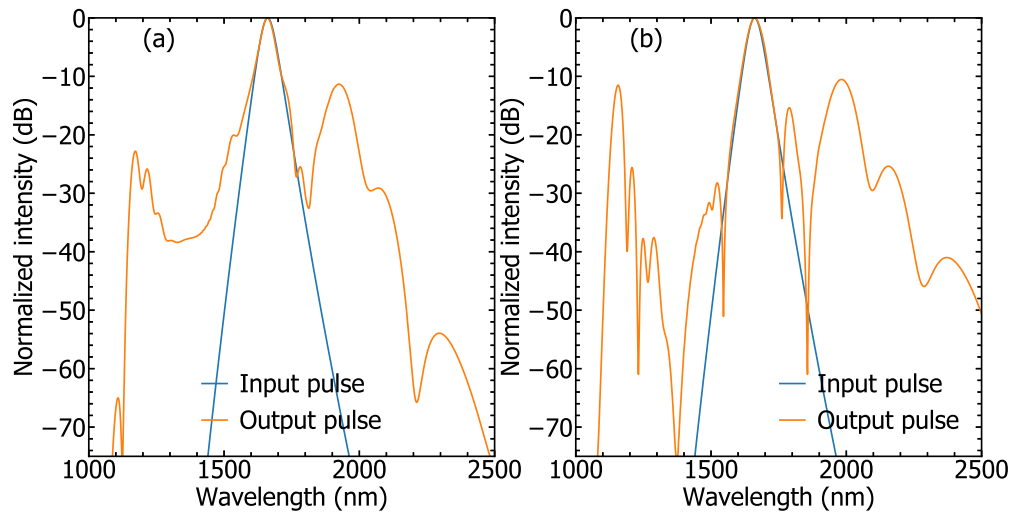
Figure 5.2 Two numerically simulated outputs with 12 nJ (a) and 14 nJ (b) respectively. The input is a theoretical Gaussian pulse with a FWHM duration of 60 fs and a central wavelength of 1660 nm, the spectra are the simulated results after 2 cm of propagation through 2004C7.
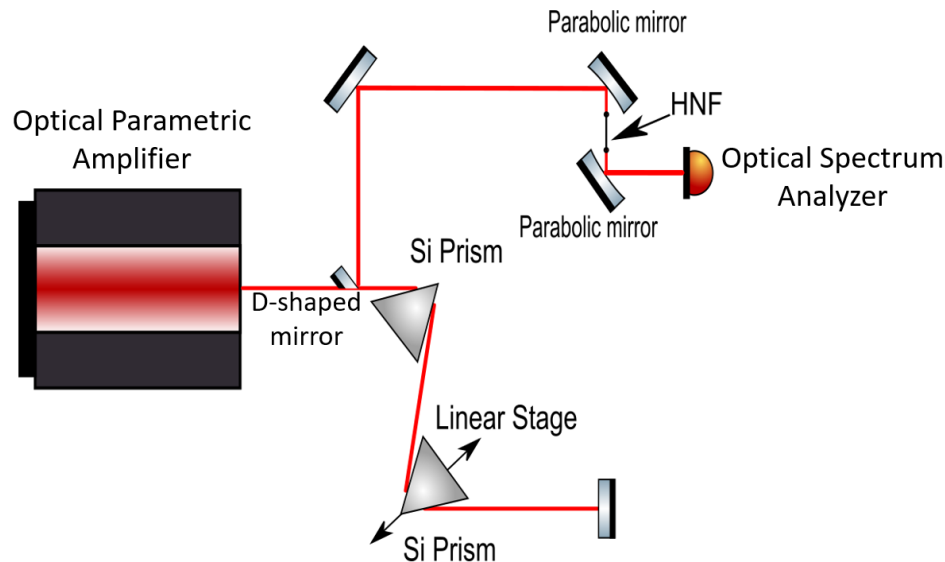
Figure 5.3 Setup to generate supercontinuum in the HNF, the beam goes through a prism pair to fine tune its dispersion at the input of the HNF it is focused into. The beam is then reflected on a D-shaped mirror. After the fiber, the beam is directed into an optical spectrum analyser.

signal with an adjustable wavelength between 1150 and 2500 nm. The pulse duration is around 60 fs and the energy before the coupling is around 10 nJ. Four compression options

are available at the end of the OPA: no crystal, a 3mm thick ZnSe, a 5mm thick ZnSe and a 10mm thick ZnSe.

The prism pair is a tool to fine tune the dispersion before going in the fiber and optimize the output spectrum.

The end of the setup is just the propagation through the fiber itself and the acquisition of the spectrum with an Optical Spectrum Analyser (OSA).

5.2.2 Acquired spectra

The OSA spans from 800 to 1750 nm. Since we are interested in studying the response of the 2004C7 fiber for wavelengths near the zero dispersion point (at 1670 nm), this means that the soliton will not be visible on the spectrum. The only part that we will be able to see is the dispersive wave.

The zero dispersion point of the fiber is at 1670 nm, the wavelengths chosen to generate supercontinuum were between 1640 and 1725 nm, as the best results for supercontinuum generation happen for a pump wavelength slightly above the zero dispersion wavelength.

There are two other adjustable parameters to influence the generation: the input energy and the GDD. The main GDD choices were done changing the crystal at the output of the OPA and the energy was lowered using ND filters.

The two criteria to evaluate the quality of the supercontinuum are its spectral bandwidth and the energy conversion from the pump to the dispersive wave.

The next few spectra are taken with an input pulse energy of 10 nJ, only varying the wavelength, Figures 5.4 and 5.5 show the supercontinuum not attenuated at 1650 and 1700 nm, respectively.

As expected, both wavelength and dispersion influence the bandwidth of the output spectrum. The best results are with an input of 1700 nm. Attenuating the power by half gives a narrower spectrum as Figure 5.6 shows.

The fraction of the power acquired by the OSA in the dispersive wave is around 20% for both the pump at 1650 and at 1700 nm (for no ZnSe crystal). It is 25.4% for 1700 and 23.1% for 1650 nm, confirming that the conversion is slightly better in the first case.

Attenuating the power only gives worst results as these two Figures show. The reason for that is probably the soliton on the other side of the pump. The condition for soliton propagation is the compensation of the dispersive effects in the fiber by the nonlinear effects. It is also the reason why picking a wavelength with a GVD slightly negative (a little above the zero

Figure 5.4 Supercontinuum spectrum with an input energy of 10 nJ and an input of 1650 nm. The 4 GDD values are the four crystal options, 0 fs^2 is the output without a crystal, 936, 1560 and 3120 fs^2 are the 3 mm, 5 mm and 10 mm ZnSe respectively.

dispersion wavelength) gives the best results. In this case, the nonlinear effects are not strong enough to compensate the dispersion in the fiber.

Figure 5.5 Supercontinuum spectrum with an input energy of 10 nJ and an input of 1700 nm. The 4 GDD values are the four crystal options, 0 fs^2 is the output without a crystal, 936, 1560 and 3120 fs^2 are the 3 mm, 5 mm and 10 mm ZnSe respectively.
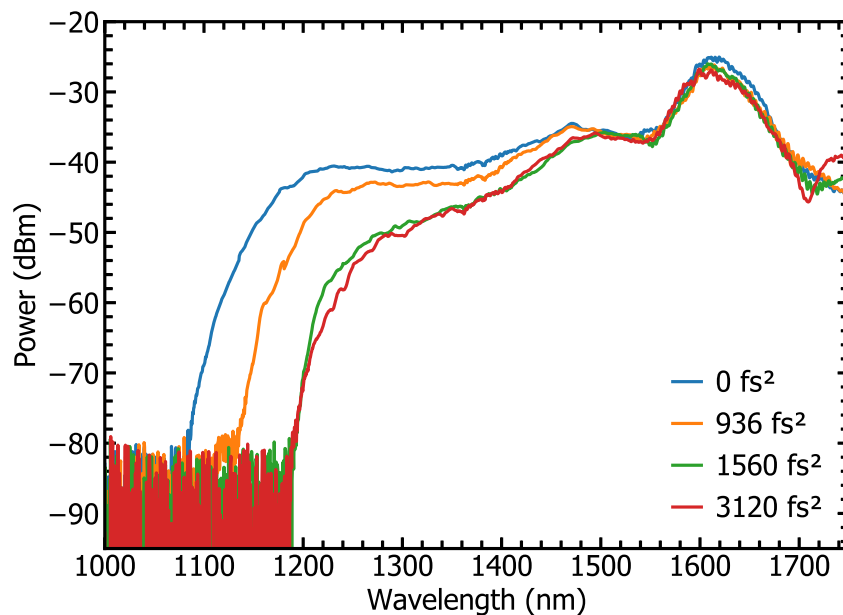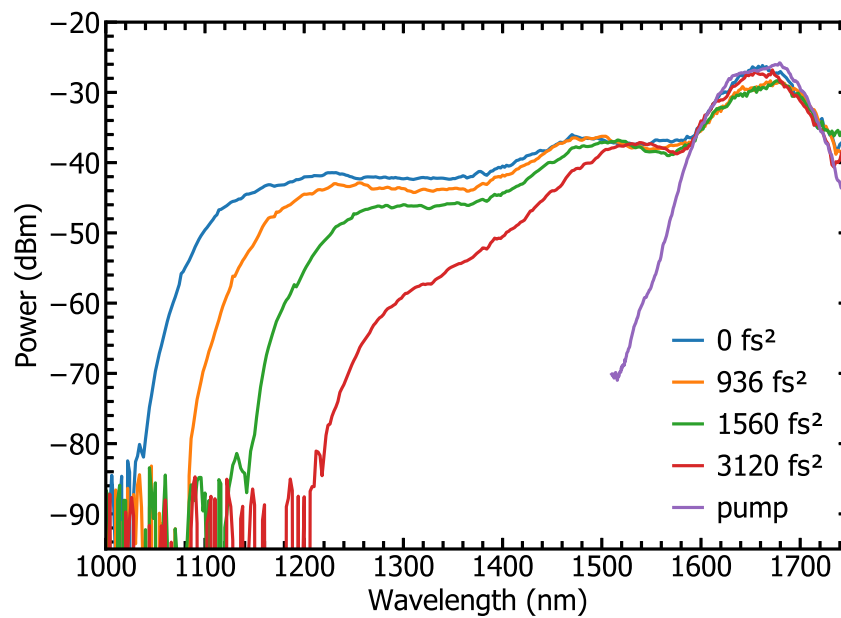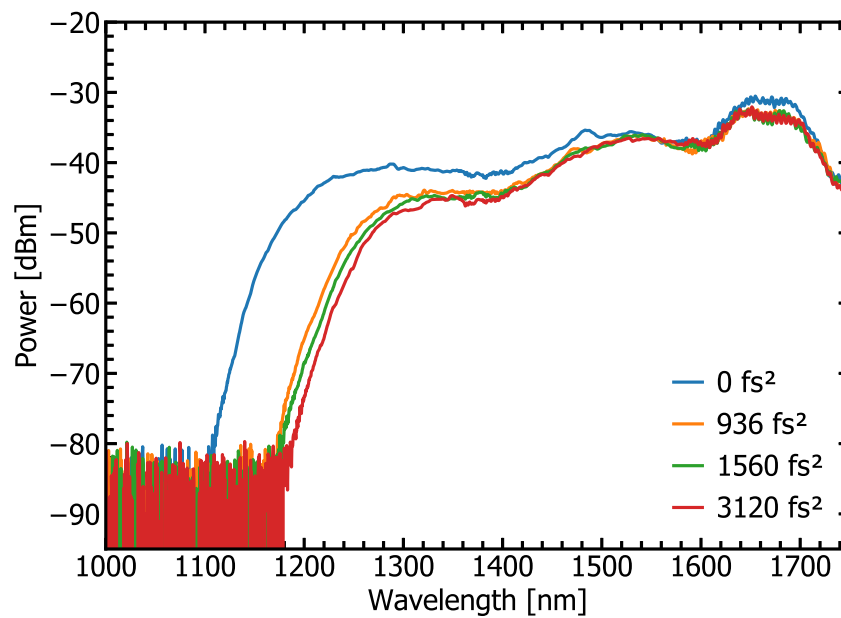
Figure 5.6 Supercontinuum spectrum with an input energy of 5 nJ and an input of 1650 nm. The 4 GDD values are the four crystal options, 0 fs^2 is the output without a crystal, 936, 1560 and 3120 fs^2 are the 3 mm, 5 mm and 10 mm ZnSe respectively.

5.2.3 Comparison with simulation

The final step of this work is to compare the simulation results showed in section (5.1.3) with the experimental results showed in the previous section. Figure 5.7 shows a comparison of experiment and simulation for an input energy of 12 nJ. As the exact phase of the experimental pulse is unknown, the GDD of the simulated pulses had to be estimated. The manufacturer of the OPA measured the pulse duration at all wavelengths for all different compression options. At the wavelength of 1660 nm, the best compression option is the 3mm ZnSe crystal. The output pulse with no ZnSe crystal then has a slightly negative GDD. Without accounting for the prism pair, its GDD is -900 fs^2, adding 500 fs^2 with the prism pair brings it to -400 fs^2. The chosen input GDD in the simulation is the same (-400 fs^2). The third order induced by the prism pair is also estimated and added to the simulated pulse. The estimated value in this case is 45000 fs^3, which is also added to the simulation input pulse.

There is an overall clear agreement between the simulated and the experimental results. In both cases, there is a clear flat dispersive wave at wavelengths lower than the pump with a sharp cut-off around 1100 nm.

In the experiment, varying the amount of dispersion on the input pulse had a direct influence on the bandwidth of the generated spectrum. Figure 5.8 shows the same comparison as in Figure 5.7 but this time with an added dispersion corresponding in the experimental setup to adding 5 mm of ZnSe. In the simulated results, the same amount of GDD and TOD was added to the input pulse.

As in the experiment, adding positive group delay dispersion generally reduces the bandwidth of the dispersive wave. This behaviour happens in both experiment and simulation.

The best results are found for an input energy of 10 nJ with no added compression. Figure 5.9 shows the resulting dispersive wave numerically filtered. The filter function is the following: $F(\lambda) = e^{-2(\frac{\lambda - \lambda_0}{\lambda_f})^8}$, where λ_0 is the center wavelength of the filter, in this case 1350 nm and λ_f is half the bandwidth of the filter, in this case 335 nm. The point of this filtering is to show the resulting bandwidth and more importantly the resulting compressed pulse duration.

The result of this filtering is a spectrum with a bandwidth of over 500 nm. The compressed duration of a pulse with this bandwidth is just below 6 fs. The energy converted in this dispersive wave is a little over 4 nJ.
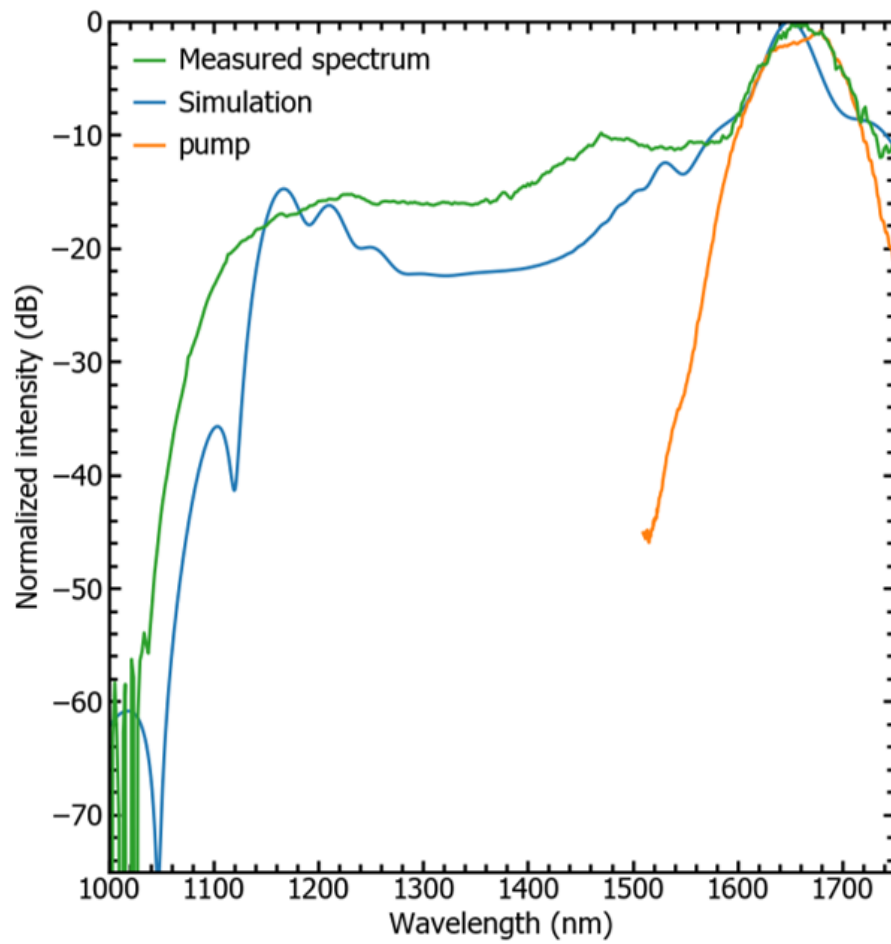
Figure 5.7 Comparison of experimental and simulated spectra. The input of the simulation is a theoretical Gaussian pulse with a FWHM duration of 60 fs and a central wavelength of 1660 nm, matching the experimental input pulse parameters.
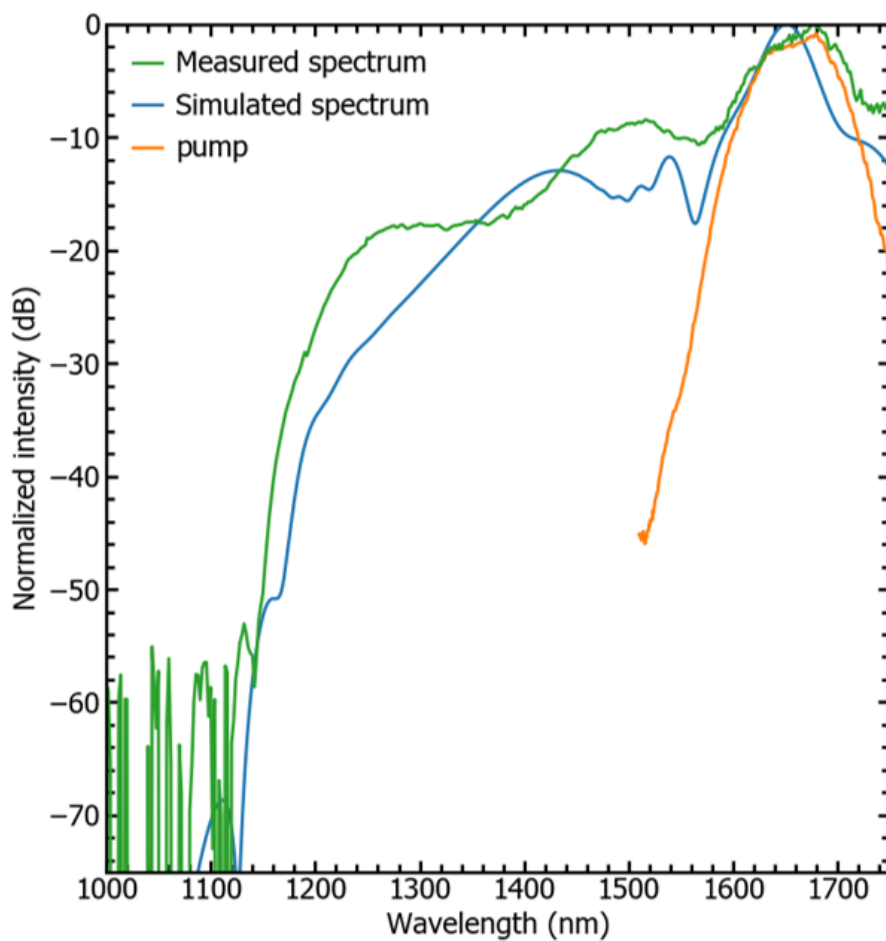
Figure 5.8 Comparison of experimental and simulated spectra. The input of the simulation is a theoretical Gaussian pulse with a FWHM duration of 60 fs and a central wavelength of 1660 nm. The input of the experiment is a 60 fs pulse with a center wavelength of 1660 nm. The experimental input goes through a 5mm thick ZnSe crystal, 1500 fs^2 of GDD and 1875 fs^3 were added to the simulated input.

Figure 5.9 Filtered amplitude spectrum of the dispersive wave with an input of 10 nJ at a wavelength of 1660 nm.

CHAPTER 6   CONCLUSION

To conclude this work, I present a summary of the work that was accomplished during the Masters, look at the limitations of it and finally discuss the options to improve the setup and take it further.

6.1   Summary of work

This work showed two major results, the characterization of the dispersion in different optical fibers and the simulation of the propagation of a pulse.

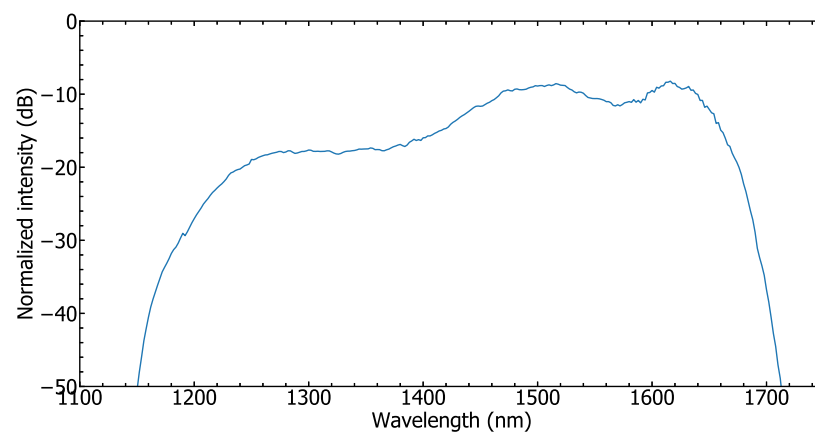### 6.1.1   Dispersion characterization

The dispersion of two fibers was characterized with a precise interferometer. The first characterized fiber was SMF28, the most used fiber in telecommunication. The objective behind the characterization of this specific fiber was to confirm that the setup worked properly. The dispersion of SMF28 is indeed well known as it is necessary to ensure its use in information transmission. The comparison between the results obtained with the interferometer and the dispersion curve given by the manufacturer confirmed the setup was working properly.

After confirming the setup gave the proper dispersion curve, another fiber was characterized. As the final objective was to use such a fiber to generate a supercontinuum, the fiber chosen was a highly nonlinear fiber with a much smaller core. Using the same method gave another dispersion curve for this fiber.

6.1.2   Supercontinuum generation

Having a dispersion curve for the highly nonlinear fiber allows to simulate effectively the propagation of a short pulse in the fiber. Using a Python simulation software, the generation of a supercontinuum was simulated in 2 cm of highly nonlinear fiber. The Python software used is the PyNLO package [39]. Reproducing the parameters used in the simulation in the laboratory allowed to observe a spectral broadening of the pulse as well. A semi-quantitative agreement was achieved between simulation and experiment, where most salient features have been quantitatively captured such as spectral broadening, overall slope of the dispersive wave in frequency as well as the magnitude and position of the abrupt high-frequency spectral cutoff. The influence of the input parameters such as energy and dispersion of the input pulse

were also explored both in simulation and in experiment. In the end, using a 60 fs pulse from the output of an industrial OPA and broadening it inside a HNF generated a spectrum with a bandwidth over 500 nm with a central wavelength of 1350 nm. This type of bandwidth supports the generation of sub 6 fs pulses, in this case with an energy a little over 4 nJ.

6.2 Limitations

Despite the project having achieved dispersion characterization and pulse propagation simulation, it still has significant limitations. The first is the frequency resolution and span of the interferometer. Another limitation is the adaptability of the setup, for instance the ability to easily change the fiber to characterize.

6.2.1 Interferometer resolution

In terms of measurement, some of the criteria to evaluate the quality of a setup are the signal to noise ratio, the resolution and the span of the setup. In this case, the SNR is limited by the vibrations in the setup, improving the quality of the optomechanics and isolating the setup would attenuate the vibrations. The resolution and the span are both limited by the source. The span we were able to achieve with this source is not enough to characterize fibers in the infrared.

6.2.2 Adaptability

One of the secondary purposes of the characterization setup was to be versatile. The setup was meant to be used to easily characterize multiple fibers. The idea was to have a portable station with a source and interferometer on a breadboard. Because of the absence of a monochromator, the source is not portable at all. On the other hand, though it is possible to change fiber, a complete alignement of the arm of the interferometer after the fiber has to be done to obtain interfences. Ideally, it should be possible to change the fiber to characterize with minimum realignments, for example the couplings mirror in and out of the fiber.

6.2.3 Simulation issues

Despite showing very similar behaviours, there are still discrepancies between simulation and experiment. This can be explained by the fact that the simulation inputs were all theoretical Gaussian pulses. They did not input an actually experimentally measured pulse.

6.3 Future research

The possible future ameliorations are mostly ways to solve or push back the limitations of the setup.

6.3.1 Interferometer resolution

There are two main ways to improve the overall quality of the measurement setup, the first one is to improve the quality of the box isolating the setup from the outside air flow. Building a box with metal posts holding plastic panels would provide better isolation than just a coroplast box. The second major way to improve the SNR is to look at individual pieces of the setup and figure out where most of the noise is coming from. The first step to this is to replace the beam splitter holders that are still made of plastic with the same pieces made of metal.

6.3.2 Adaptability

The main feature missing from the interferometer is the ability to change fibers easily. To do so, having a single mount to hold the fiber with 6 axis stages at both ends of the fiber would theoretically allow for an easier change of fiber. The other big change that needs to be done is to make the setup completely portable. To do so, the source needs to be changed, the best option for this change is to take a tungsten filament source. This kind of lamp could be clamped to the breadboard and transported. However, using a tungsten white source would remove the possibility to adjust the wavelength at the input of the setup. To solve this, a monochromator could be added at the end of the interferometer to select a specific wavelength. The quality of the monochromator is the limitation factor to the wavelength resolution.

6.3.3 Simulation

A crucial step to improve the simulation results would be to measure the spectral amplitude and phase of the input pulse. A measurement setup like a FROG or a SPIDER is ideal for this kind of analysis. These setups are able to retrieve the phase of an ultrashort pulse. Having the exact data for the input pulse would make the simulation much more accurate and relevant. Instead of manually inputing a quadratic phase, it would be possible to simulate the exact input phase. Further exploration of the simulation space is also necessary. Finding more precise energy and dispersion parameters in the simulation would further increase agreement between simulation and experiment.

REFERENCES

[1] "Zernike polynomials," in *Wikipédia*, 30 nov. 2019. [Online]. Available: https//en. wikipedia.org/wiki/Zernike_polynomials#/media/FileZernike_polynomials2.png

[2] P. W. Smith, "Mode-locking of lasers," *Proceedings of the IEEE*, vol. 58, no. 9, pp. 1342–1357, Sep. 1970.

[3] T. Deutsch, "Mode-locking effects in an internally modulated ruby laser," *Applied Physics Letters*, vol. 7, no. 4, pp. 80–82, 1965.

[4] U. Keller *et al.*, "Femtosecond pulses from a continuously self-starting passively mode-locked ti: sapphire laser," *Optics letters*, vol. 16, no. 13, pp. 1022–1024, 1991.

[5] G. D. Tsakiris *et al.*, "Route to intense single attosecond pulses," *New Journal of Physics*, vol. 8, pp. 19–19, jan 2006. [Online]. Available: https: //doi.org/10.1088%2F1367-2630%2F8%2F1%2F019

[6] G. Sansone *et al.*, "Isolated single-cycle attosecond pulses," *Science*, vol. 314, oct 2006.

[7] R. Trebino *et al.*, "Measuring ultrashort laser pulses in the time-frequency domain using frequency-resolved optical gating," *Review of Scientific Instruments*, vol. 68, no. 9, pp. 3277–3295, 1997.

[8] C. Iaconis and I. A. Walmsley, "Spectral phase interferometry for direct electric-field reconstruction of ultrashort optical pulses," *Optics letters*, vol. 23, no. 10, pp. 792–794, 1998.

[9] R. H. Stolen and C. Lin, "Self-phase-modulation in silica optical fibers," *Phys. Rev. A*, vol. 17, pp. 1448–1453, Apr 1978. [Online]. Available: https: //link.aps.org/doi/10.1103/PhysRevA.17.1448

[10] W. J. Tomlinson, R. H. Stolen, and C. V. Shank, "Compression of optical pulses chirped by self-phase modulation in fibers," *J. Opt. Soc. Am. B*, vol. 1, no. 2, pp. 139–149, Apr 1984. [Online]. Available: http://josab.osa.org/abstract.cfm?URI=josab-1-2-139

[11] A. M. Zheltikov, "Let there be white light: supercontinuum generation by ultrashort laser pulses," *Physics-Uspekhi*, vol. 49, no. 6, p. 605, 2006. [Online]. Available: https://doi.org/10.1070%2Fpu2006v049n06abeh005975

[12] V. I. Talanov, "Self focusing of wave beams in nonlinear media," *JETP Lett.*, pp. 138–141, 1965.

[13] T. Brabec *et al.*, "Kerr lens mode locking," *Opt. Lett.*, vol. 17, no. 18, pp. 1292–1294, Sep 1992. [Online]. Available: http://ol.osa.org/abstract.cfm?URI=ol-17-18-1292

[14] J. Herrmann, "Theory of kerr-lens mode locking: role of self-focusing and radially varying gain," *J. Opt. Soc. Am. B*, vol. 11, no. 3, pp. 498–512, Mar 1994. [Online]. Available: http://josab.osa.org/abstract.cfm?URI=josab-11-3-498

[15] T. G. Giallorenzi, "Optical communications research and technology: Fiber optics," *Proceedings of the IEEE*, vol. 66, no. 7, pp. 744–780, July 1978.

[16] H. Coddington, *A Treatise on the Reflection and Refraction of light: being Part I. of a System of Optics*, 1829.

[17] G. P. Agrawal, "Nonlinear fiber optics," in *Nonlinear Science at the Dawn of the 21st Century.* Springer, 2000, pp. 195–211.

[18] D. Marcuse, "Interdependence of waveguide and material dispersion," *Applied optics*, vol. 18, no. 17, pp. 2930–2932, 1979.

[19] R. Kashyap, *Fiber Bragg gratings.* Academic press, 2009.

[20] H. Nakatsuka, D. Grischkowsky, and A. Balant, "Nonlinear picosecond-pulse propagation through optical fibers with positive group velocity dispersion," *Physical Review Letters*, vol. 47, no. 13, p. 910, 1981.

[21] C. Burrus *et al.*, "Pulse dispersion and refractive-index profiles of some low-noise multimode optical fibers," *Proceedings of the IEEE*, vol. 61, no. 10, pp. 1498–1499, 1973.

[22] K. Thyagarajan *et al.*, "A novel design of a dispersion compensating fiber," *IEEE photonics technology letters*, vol. 8, no. 11, pp. 1510–1512, 1996.

[23] T. Birks *et al.*, "Dispersion compensation using single-material fibers," *IEEE Photonics Technology Letters*, vol. 11, no. 6, pp. 674–676, 1999.

[24] L. Grüner-Nielsen *et al.*, "Dispersion compensating fibers," *Optical Fiber Technology*, vol. 6, no. 2, pp. 164–180, 2000.

[25] R. Fork, O. Martinez, and J. Gordon, "Negative dispersion using pairs of prisms," *Optics Letters*, vol. 9, no. 5, pp. 150–152, 1984.

[26] M. Zavelani-Rossi *et al.*, "Pulse compression over a 170-thz bandwidth in the visible by use of only chirped mirrors," *Optics Letters*, vol. 26, no. 15, pp. 1155–1157, 2001.

[27] S. Diddams and J.-C. Diels, "Dispersion measurements with white-light interferometry," *JOSA B*, vol. 13, no. 6, pp. 1120–1129, 1996.

[28] L. Cohen, "Comparison of single-mode fiber dispersion measurement techniques," *Journal of lightwave technology*, vol. 3, no. 5, pp. 958–966, 1985.

[29] D. T. Delpy *et al.*, "Estimation of optical pathlength through tissue from direct time of flight measurement," *Physics in Medicine & Biology*, vol. 33, no. 12, p. 1433, 1988.

[30] L. Cherbi, M. Mehenni, and R. Aksas, "Experimental investigation of the modulation phase-shift method for the measure of the chromatic dispersion in a single-mode fiber coiled on a covered spool," *Microwave and Optical Technology Letters*, vol. 48, no. 1, pp. 174–178, 2006.

[31] P. Hamel *et al.*, "Optical low-coherence reflectometry for complete chromatic dispersion characterization of few-mode fibers," *Optics Letters*, vol. 32, no. 9, pp. 1029–1031, 2007.

[32] M. A. Galle, *Single-arm 3-wave interferometer for measuring dispersion in short lengths of fiber.* University of Toronto, 2007.

[33] L. Thevenaz, J.-P. Pellaux, and J.-P. Von der Weid, "All-fiber interferometer for chromatic dispersion measurements," *Journal of lightwave technology*, vol. 6, no. 1, pp. 1–7, 1988.

[34] L. N. Binh, "Optical fiber communication systems with matlab and simulink models," 2014.

[35] M. Premaratne and G. P. Agrawal, *Light propagation in gain media: optical amplifiers.* Cambridge University Press, 2011.

[36] Thorlabs. (2016) Sls202l - stabilized fiber-coupled ir light source w/ universal power adapter, 450 - 5500 nm, 1/4"-20 taps. [Online]. Available: https://www.thorlabs.com/thorproduct.cfm?partnumber=SLS202L

[37] LightCon. Broad bandwidth hybrid optical parametric amplifier. [Online]. Available: http://www.lightcon.com/Product/ORPHEUS-F.html

[38] PI. V-508 pimag® precision linear stage. [Online]. Available: https://www.pi-usa.us/en/products/positioning-stages-linear-rotary-motorized-precision/precision-motorized-linear-stages/v-508-pimag-precision-linear-stage-1200210/

[39] G. Ycas. (2015) pynlo, nonlinear optics modeling for python. [Online]. Available: https://pynlo.readthedocs.io/en/latest/index.html

[40] P. R. Barbier *et al.*, "Schack-hartmann wavefront sensing measurements of near-ground propagated laser beams," in *Propagation and Imaging through the Atmosphere*, vol. 3125. International Society for Optics and Photonics, 1997, pp. 284–295.

APPENDIX A   SHACK-HARTMANN SENSOR

Because of the critical significance of the beam collimation to observe interference, a Schack-Hartmann sensor was used to optimize the beam wavefronts [40]. The purpose of this sensor is to visualize the wavefront of an incoming beam. This can be used to collimate a beam, focus a beam and for all alignement processes.
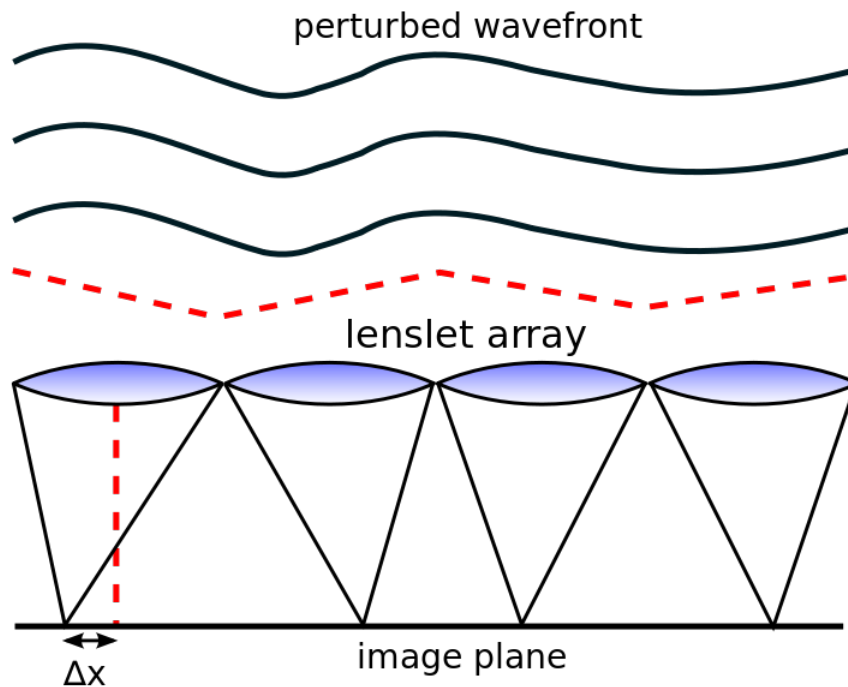

Figure A.1 1D diagram of a Shack Hartmann sensor. The sensor is an array of lenses that focus incoming light to a camera.

The sensor is made of an array of microlenses that have their focal point on a camera, as shown in figure A.1.

Shining a beam on this type of sensor gives a matrix of light points like figure A.2 shows.

All the information about the shape of the wavefront is contained in the position of these points. Assuming the wavefront is perfectly flat and the sensor is perfect, the picture acquired by the camera would be a perfect grid of points. As figure A.1 shows, a perturbed wavefront offsets the light points from their perfect position.

In order to retrieve the wavefront shape, the first required step is to get the offset between the light points on the camera and their position in a perfect wavefront. The position of the
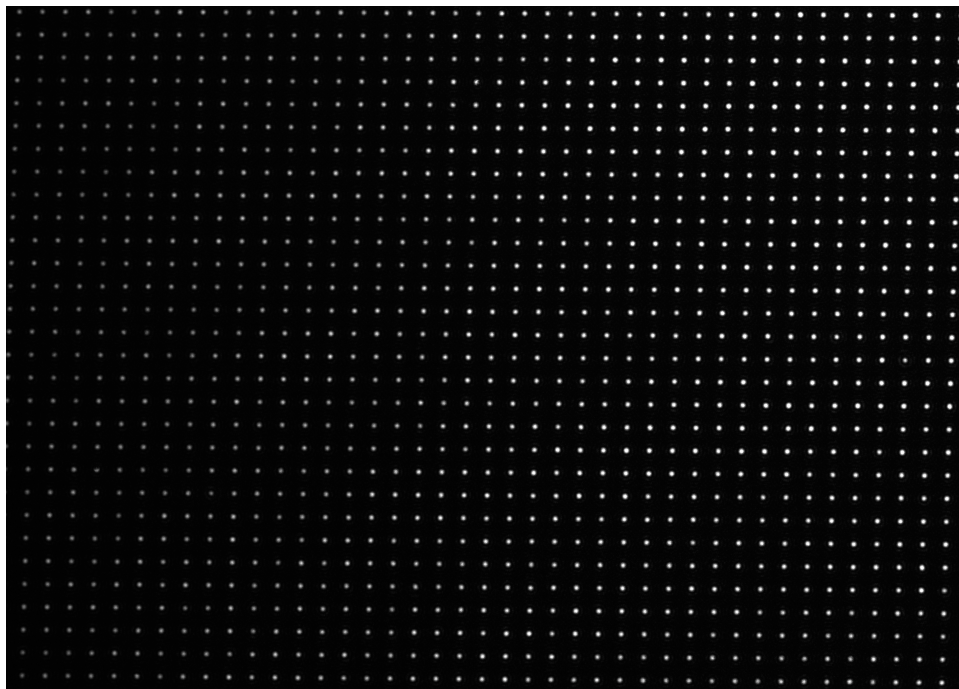
Figure A.2 Example of picture acquired by the sensor

points in the picture is easy to find, the harder part is to extrapolate the theoretical positions of the points for a perfect wavefront. These points are simply the focal points of the lenses of the lens matrix. One of the way to get these positions would be to have a perfect wavefront available to shine on the sensor. Unfortunately, such a wavefront does not exist in reality, so as an alternative, the other option is to fit a grid on the acquired picture.

Finding the positions of all the points in the picture and creating a grid of squares gives a good approximation for the real positions of the focal points. After creating such a grid, the offset needed to describe the wavefront simply is the vector linking the light point on the picture with its relative grid point.

Figure A.3 shows what a grid of focal points looks like. The important information to extract from this kind of picture is the map of the vectors from the light points to the grid points. Figure A.4 shows these vectors with an amplified magnitude (factor 10) to make them appear more clearly.

This picture already gives a good idea about the shape of the wavefront and the type of misalignement in the beam. In this case the $\vec{k}$ vectors seem to be rotating around a point in the middle of the lower part of the sensor.

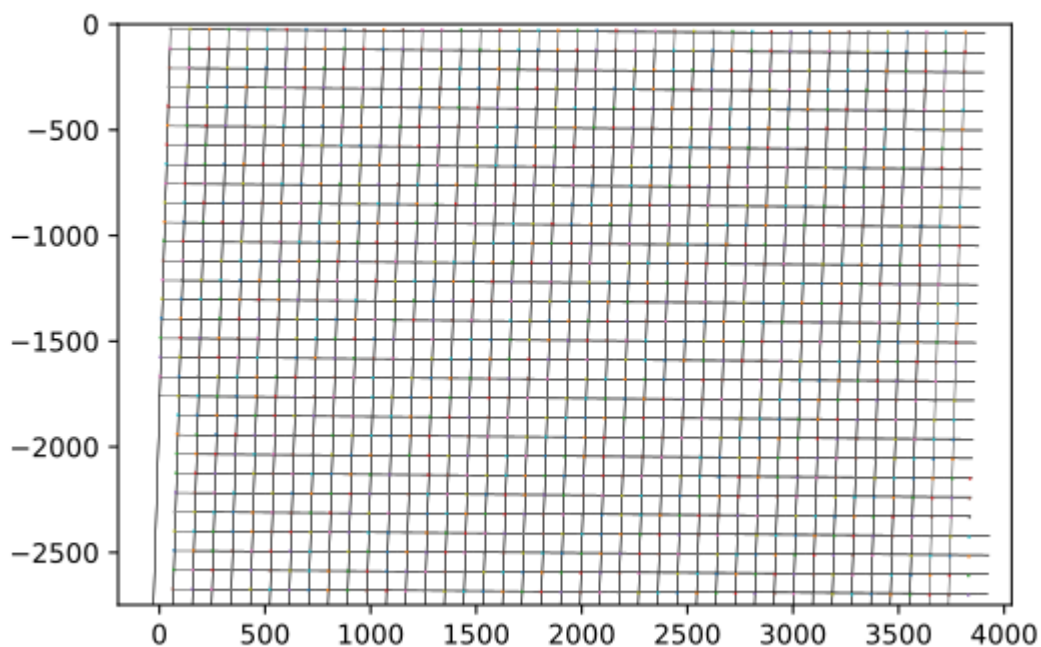This kind of picture can already be used for alignement, as it gives a quantitative way to view

Figure A.3 Processed image with a plotted grid

the defaults. It can be used to identify a collimated beam, where all the $\vec{k}$ vectors would be parallel, so the points would perfectly overlap the grid. For a focusing beam, the $\vec{k}$ vectors would all be pointing toward the same point, for a defocusing beam, they would all point away from the same point.

Even if this kind of wavefront description gives a lot of information, there is a better way to quantify the defaults of the beam. Decomposing the vector map in a polynomial base gives even more information than the vectors themselves. The perfect base for this is a group of polynomial functions called the Zernike polynomials. They form a base of the 2D vector space we are trying to decompose.

These polynomial functions are especially interesting as they can be linked to known optical beam defaults. Figures A.5, A.6 and A.7 show three examples of these functions.

Figure A.5 is the second Zernike function, it is the simplest degree 1 polynomial, just a tilt. The third is also a tilt, but in the other direction.

The fourth polynomial (figure A.6) corresponds to a focusing beam, or a defocusing beam depending on the sign.
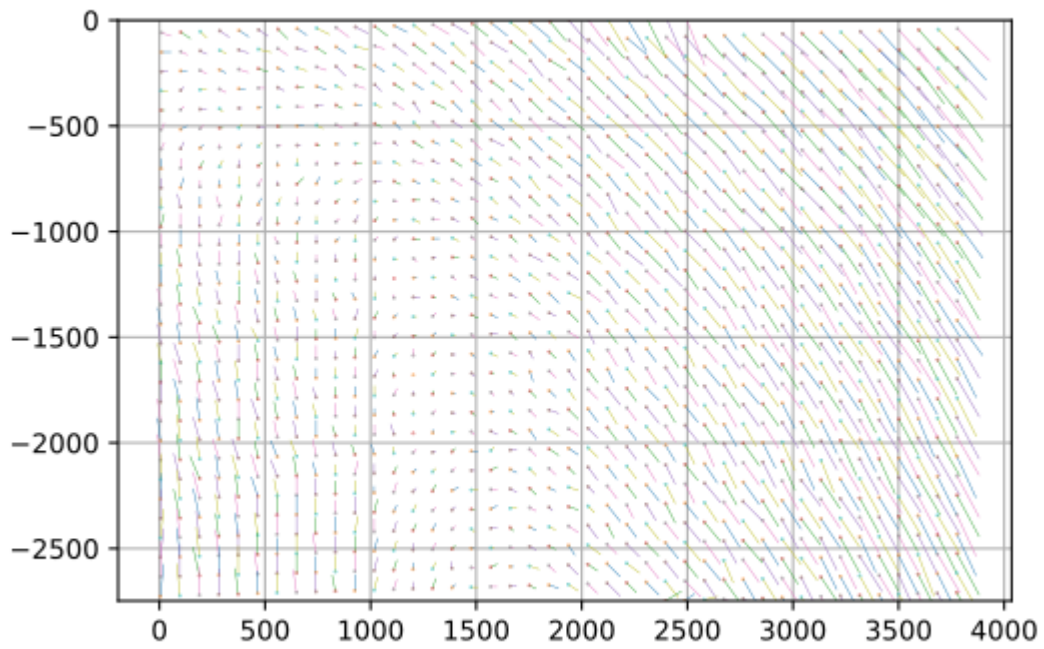
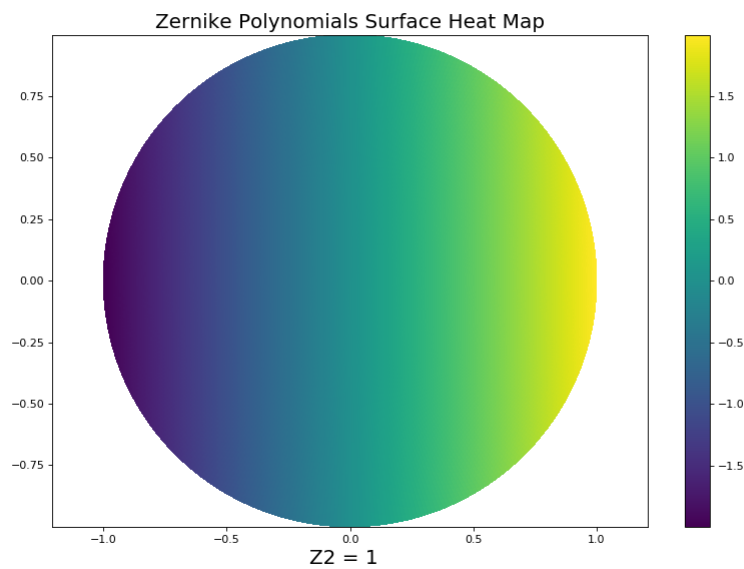Figure A.4 Vectors between the light points and the grid points

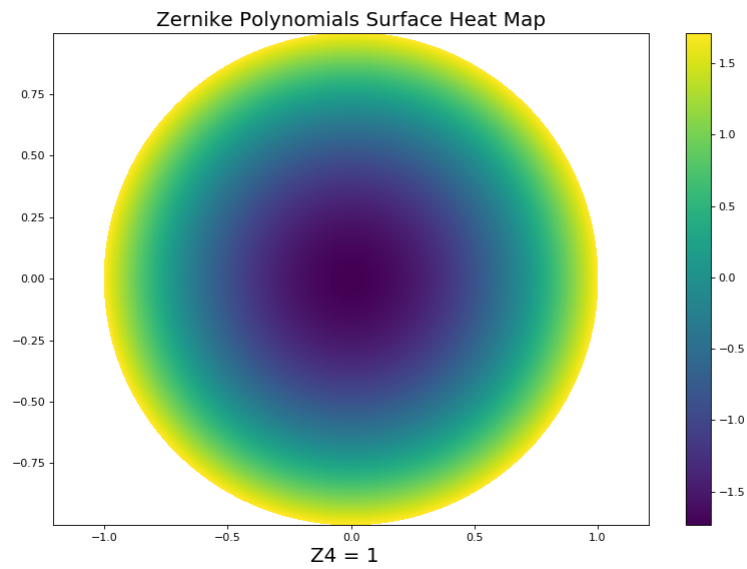Figure A.5 Zernike polynomial number 2

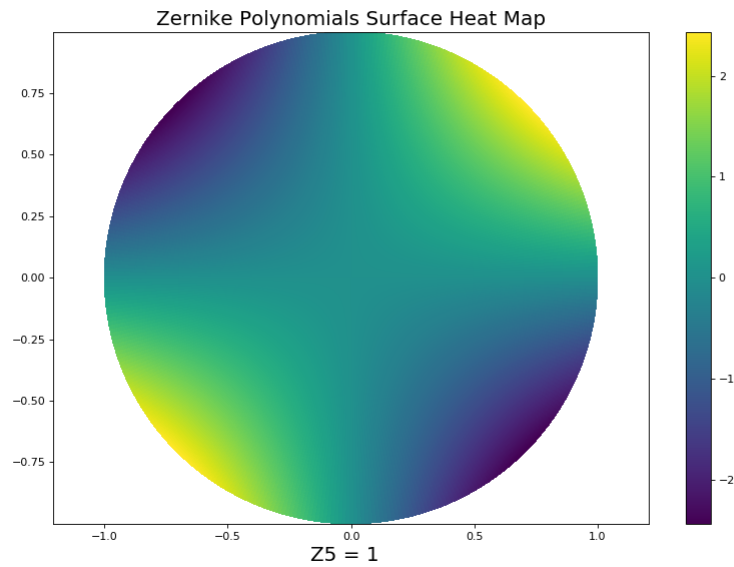Figure A.6 Zernike polynomial number 4

Figure A.7 Zernike polynomial number 5

The fifth Zernike polynomial (figure A.7) is a combination of two defaults, the first one is again a focus, but the second one is much more interesting and harder to detect, it is astigmatism.

The seventh polynomial is a combination of coma and tilt. Polynomials with a degree higher than 3 become combinations of more defaults and are then much harder to decribe.

Another thing to note is the number of the polynomials. This does not corerspond to the degree of the polynomial but to its index. Figure A.8 shows the first 21 functions and their degree.
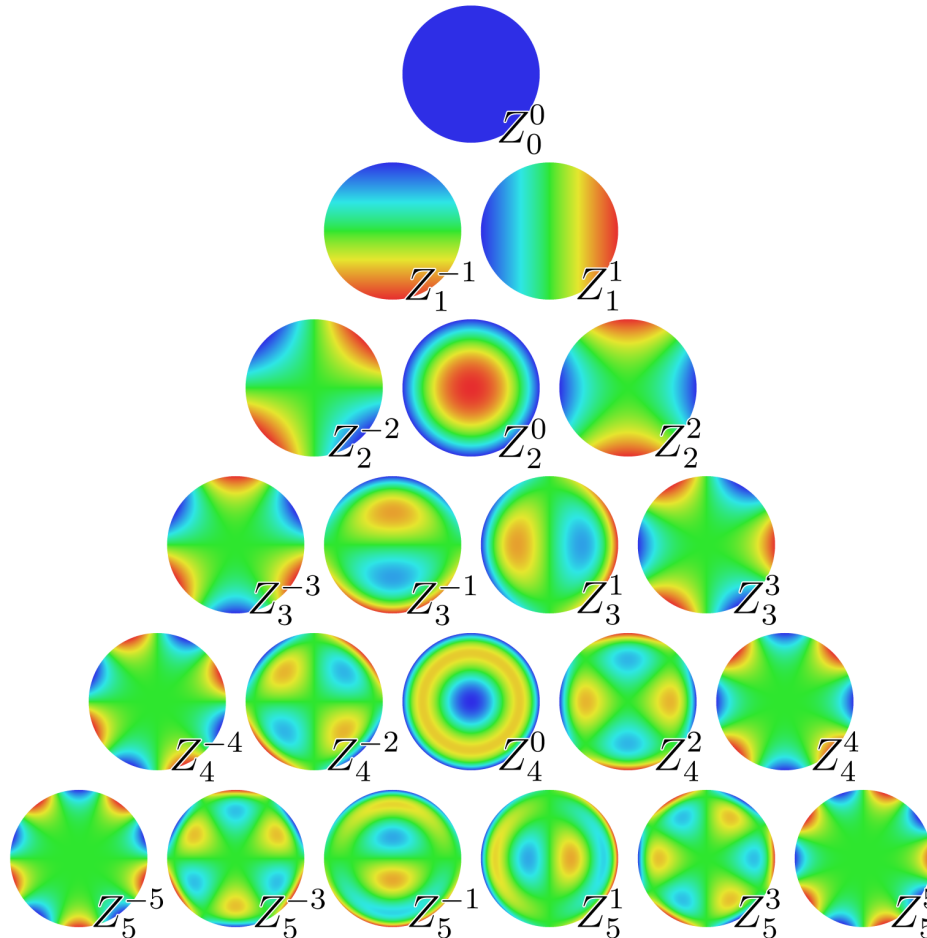

Figure A.8 Zernike polynomial up to the 21st, covering degrees 0 to 4 [1].

Having these functions as a base of the 2D vector space allows us to decompose the vector field into these polynomials. Doing so gives a coefficient to each of the Zernike functions and quantifies each of the defaults of the incoming beam on the sensor. Identifying the type of misalignement helps to know how to realign more efficiently.